JOURNAL OF GEOPHYSICAL RESEARCH, VOL. 94, NO. D14, PAGES 16,815–16,845, NOVEMBER 30, 1989

Reconstruction of the Constituent Distribution and Trends in the Antarctic Polar Vortex From ER-2 Flight Observations

MARK R. SCHOEBERL,[1] LESLIE R. LAIT,[1] PAUL A. NEWMAN,[2] RUSSELL L. MARTIN,[2]
MICHAEL H. PROFFITT,[3] DENNIS L. HARTMANN,[4] MAX LOEWENSTEIN,[5]
JAMES PODOLSKE,[5] SUSAN E. STRAHAN,[5] JAMES ANDERSON,[6]
K. ROLAND CHAN,[5] AND BRUCE GARY[7]

During the Airborne Antarctic Ozone Experiment, the high-altitude ER-2 aircraft measured ozone, chlorine monoxide, and nitrous oxide concentrations in the south polar region. These measurements have been analyzed using conservative coordinate transformations to potential temperature–N_2O and potential temperature–potential vorticity space. The latter transformation is equivalent to interpreting trace species observations within the modified Lagrangian mean (MLM) coordinate system. With certain assumptions about zonal symmetry, this transformation allows for the interpretation of chemical changes of constituents independent of meteorological variability. The method also allows for a reasonable reconstruction of constituent distributions outside the aircraft flight track. Our analysis shows that the MLM transformed ozone concentration decreases at about 0.06 ppmv (parts per million by volume) per day between 20 and 16 km altitude inside the polar vortex during the mid-August to mid-September period. These ozone changes must be chemical in origin; they are also collocated with the region of high ClO. Outside the CPR (chemically perturbed region) at the highest aircraft altitudes, ozone systematically increases, suggesting a diabatic cooling of the order of 0.3–0.6 K/d. Within the CPR the cooling rate appears to be less than 0.2 K/d. The MLM analysis technique creates a picture of the general chemical structure of the Austral polar vortex which shows that air deep within the chemically perturbed region has subsided substantially in relation to the air outside. However, there is also a tongue of high ozone air which extends from mid-latitudes downward along the stratospheric jet at 65°W and 60°S. An examination of the last three flight days, September 20–22, 1987, shows that during this period the polar vortex shifts systematically equatorward along the Antarctic Peninsula. Apparent changes in the constituents measured over this period result from sampling air progressively further into the vortex.

1. INTRODUCTION

The Airborne Antarctic Ozone Experiment (AAOE) was designed to determine the cause of the spring decline in Antarctic total ozone. Thirteen flights of the NASA high-altitude ER-2 research aircraft were made from Punta Arenas, Chile (53°S, 71°W), during August and September 1987, with 12 flights penetrating the poleward side of the subpolar stratospheric jet (the polar vortex) into the chemically perturbed region (CPR). The southernmost leg of each flight usually terminated near the base of the Antarctic Peninsula, where the ER-2 dived to lower altitudes to obtain vertical profiles of constituent distributions. The flight paths covered roughly the same geometric volume, so the observations, for many purposes, can be considered spatially fixed.

The two major hypotheses which AAOE was designed to test were the chlorine chemical destruction mechanism (see *Solomon* [1988] for a review of proposed mechanisms prior to AAOE) and the dynamical upwelling mechanism [*Tung*, 1986; *Mahlman and Fels*, 1986; *Rosenfield et al.*, 1988]. To test these hypotheses and to examine the overall characteristics of the Antarctic stratosphere, the ER-2 was equipped with instruments to measure the minor constituents ozone, chlorine monoxide, bromine monoxide, nitrous oxide, NO, or NO_y, as well as winds, pressure, temperature, and the lapse rate. In this paper the structure and evolution of chlorine monoxide, ozone, nitrous oxide, water vapor, and the meteorological fields will be considered.

Even prior to the AAOE mission, ground-based and balloon observations indicated that the stratospheric air over Antarctica was chemically perturbed. The 1986 National Ozone Expedition NOZE found evidence for unusually high levels of active chlorine compounds in the region of the ozone depletion [*De Zafra et al.*, 1987; *Solomon et al.*, 1987]. Furthermore, south pole ozonesondes reported by *Kohmyr et al.* [1988] indicated significant notching of the ozone profile well within the vortex, not generally consistent with the dynamically driven upwelling mechanism [*McIntyre*, 1988]. Despite the circumstantial evidence provided by these investigations, in situ observations were needed to pin down the details of the chemical and dynamical processes taking place within the Austral polar vortex.

Even though the Austral winter circumpolar vortex is less disturbed than its boreal counterpart, disturbances to the vortex are sufficient to produce transient fluctuations in trace gas measurements made at fixed locations. Most of these fluctuations are attributable to the bodily shifting of the vortex (through the interaction with planetary-scale Rossby waves), while others are attributable to the small-scale features presumably produced by Rossby-wave breaking or folding [e.g., *McIntyre and Palmer*, 1983]. During some ER-2 missions (notably on September 22, 1987), inner vortex or CPR air moved up the Antarctic Peninsula fairly close to

[1]NASA Goddard Space Flight Center, Greenbelt, Maryland.
[2]Applied Research Corporation, Landover, Maryland.
[3]NOAA Aeronomy Laboratory, Boulder, Colorado.
[4]Department of Atmospheric Sciences, University of Washington, Seattle.
[5]NASA Ames Research Center, Moffett Field, California.
[6]Harvard University, Cambridge, Massachusetts.
[7]Jet Propulsion Laboratory, Pasadena, California.

Paper number 89JD01013.
0148-0227/89/89JD-01013$05.00

Punta Arenas near the southern tip of the South American continent. On other days (September 20, 1987, for example) the ER-2 barely penetrated the vortex. Because of the motion of the vortex, the ER-2 observations show considerable day-to-day fluctuations. In other words, at a fixed location along the ER-2 flight track, the rms deviation of a constituent from its time mean is often large.

The fluctuations resulting from the vortex motion complicate the estimates of trends and assessment of chemical and dynamical observations. If the data could be transformed into a coordinate system that approximately follows the vortex as a material entity, then the interpretation of the data should be more straightforward. To accomplish such a transformation, air parcels must be labeled by conservative quantities which provide good tracers of motion (e.g., a tracer with a reasonably large spatial gradient is required, so that parcels from different locations can be distinguished observationally).

Lower stratospheric ozone is usually a good tracer, but it is not a suitable coordinate in this case for the obvious reason that it may be evolving chemically. Potential temperature (PT), nitrous oxide (N_2O), and potential vorticity (PV) all make suitable conservative coordinates for air parcels. PV and N_2O, however, provide more or less redundant information about the ensemble; they are, in effect, nearly degenerate references, as will be shown below. The (PT, N_2O) or (PT, PV) coordinate reference frames are, in a crude sense, vortex coordinates. By transforming into the reference frame of the vortex, the rms deviation associated with vortex motion should be reduced. In a broader sense, (PT, N_2O) or (PT, PV) comprises a Lagrangian system that moves with the ensemble of air parcels. Thus the chemical evolution of the air parcels can be better assessed.

The use of (PT, PV) as a material coordinate system was discussed first by *McIntyre* [1980]; it is a natural outgrowth of the Lagrangian mean description of atmospheric motion [*Andrews and McIntyre*, 1978] and was developed principally to overcome the topological problems associated with reinitialization of the Lagrangian mean system. The (PT, PV) system is referred to as the modified Lagrangian mean (MLM). The first practical application of the method appears in the work by *Dunkerton et al.* [1981] as an analysis of a model-simulated sudden stratospheric warming. They found that the MLM and Lagrangian mean methods appeared to agree reasonably well, despite the fact that the numerical model they used did not exactly conserve potential vorticity.

Butchart and Remsberg [1986] and *Butchart* [1987], following the suggestion of *McIntyre and Palmer* [1983], used MLM ideas to examine the conservation of constituent fields and PV within the stratosphere. Their objective was to examine polar vortex erosion by computing the area enclosed by contours of satellite-measured trace constituents and PV on PT surfaces. Since the horizontal resolution of the satellite-retrieved fields is low, they argued that most of the nonconservation of area results from the formation of thin material filaments. These filaments would then appear to vanish as their scale decreased below the resolution of the satellite instrument. The formation of filaments would be greatest near the steep gradients in potential vorticity at the edge of the winter polar vortex, as has been demonstrated with high resolution models of the barotropic equivalent to the polar vortex [*Juckes and McIntyre*, 1987].

The *Butchart and Remsberg* [1986] study and an earlier analysis by *Leovy et al.* [1985] showed that the evolution of chemically conservative tracers could more easily be interpreted using potential vorticity as a tracer of the motion. Indeed, Leovy et al. showed that the spatial evolution of ozone mirrored the evolution of the potential vorticity field. The results of Leovy et al. verify the utility of the MLM coordinate system. The two major disadvantages of MLM are (1) that potential vorticity is a quantity computed from dynamical observations and therefore subject to observational error and (2) that the potential temperature will exhibit systematic nonconservation through diabatic processes and frictional processes. This latter problem becomes especially important for analysis on a seasonal time scale [*Butchart*, 1987].

In this paper, the independent coordinates (PT, N_2O) and (PT, PV) will be used to analyze tracer fields. While not perfectly conservative, both PT and PV probably change slowly over the mission period. *Rosenfield et al.* [1988] and *Shine* [1986] show that deep inside the vortex during the August–September period the diabatic heating rate (H) is of the order of -0.2 K/d. At the subpolar edge of the vortex, H may be larger, but a small drift in PT should not significantly affect our results. Frictional sources of PV are believed to be small in the lower stratosphere. Nitrous oxide has a lifetime greater than 10 years below 30 km [*Brassuer and Solomon*, 1986]. Thus (PT, N_2O) and (PT, PV) should be sufficiently conservative references over the mission period.

Since N_2O and temperature were directly measured by the ER-2, it is relatively straightforward to construct a composite picture of the concentrations in the (PT, N_2O) reference frame. A more difficult (but potentially more useful) transformation is to place the data into (PT, PV) coordinates. The (PT, PV) transform is more useful because global computations of PV and PT from satellite-retrieved fields can be used to estimate parcel positions even when they have moved outside the ER-2 measurement range. This allows us to transform back and forth from (PT, PV) space to physical space (latitude, longitude, height coordinates) at any time, provided we can assume that the constituent has a small variance in (PT, PV) space. In other words, it is assumed that most of the time variance of the constituent with respect to a fixed point is due to the variation of PV (or N_2O) and PT with respect to that point. This assumption is supported by the observational study of *Leovy et al.* [1985] and will be discussed further below.

For slowly changing, chemically active, species, if more than one measurement of an air parcel's chemical content can be made in the conservative reference frame, then linear trend analysis can be used to estimate changes and fill in temporal gaps in the measurements. Surprisingly, this method provides a fairly complete picture of the chemical evolution and structure of the Austral polar vortex from the 10 ER-2 flights made starting August 23, 1987.

This paper presents a preliminary study of the AAOE data using the techniques described above. In section 2 the methodology and data sets used are briefly described. In section 3, transformations and trend analysis in the (PT, N_2O) and (PT, PV) reference frames are presented. An inverse transform technique is then used to reconstruct the last 3 days of the mission (September 20–22, 1987) and September 23, 1987. The final section presents our conclusions.

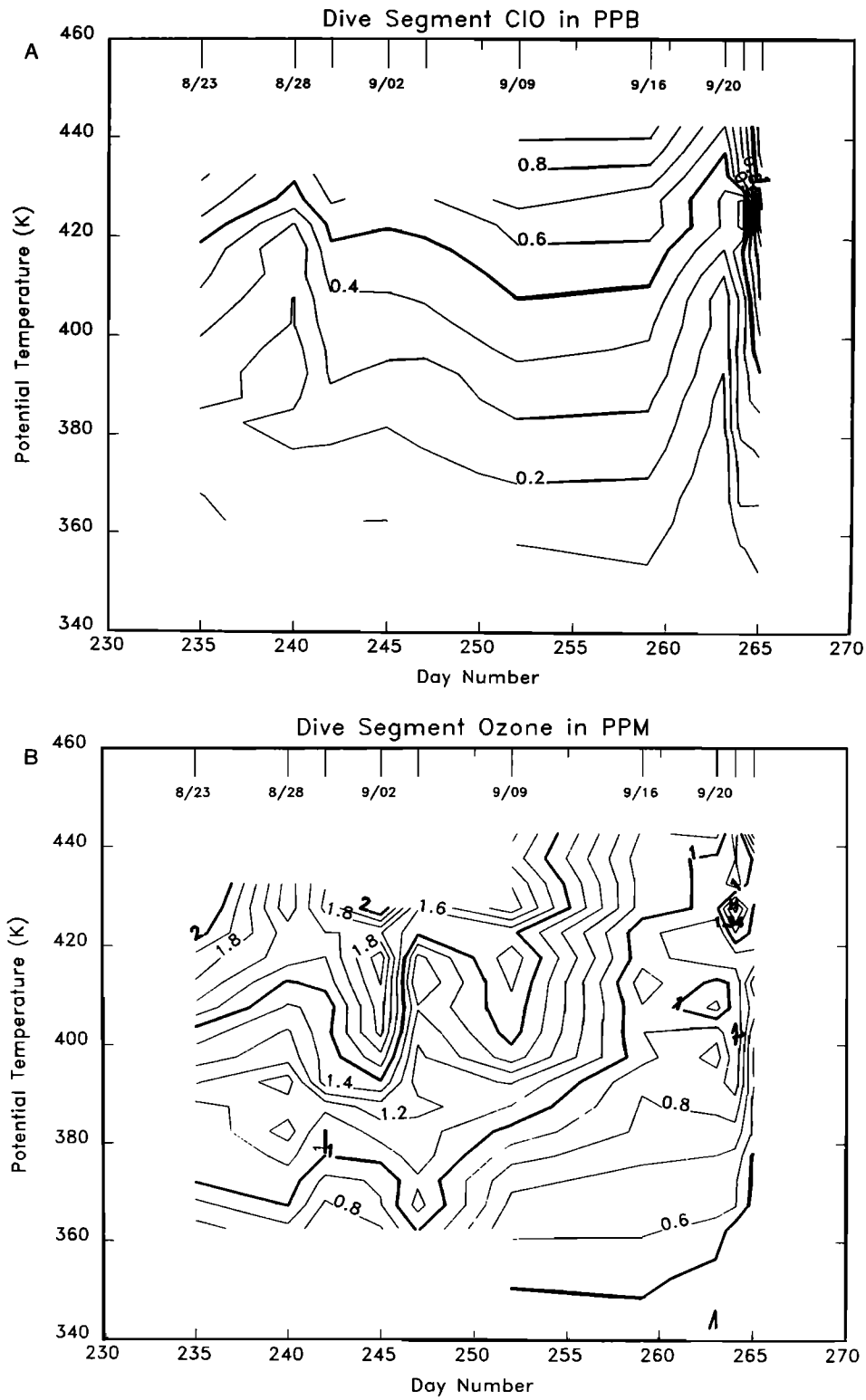

Fig. 1. A time series of (*a*) ClO, (*b*) O_3, (*c*) H_2O, and (*d*) N_2O concentration versus potential temperature from the ER-2 dives at the southern end of each flight. Flight days are marked by long ticks at the top of the figure; dates for some of the flights are also shown.

2. METHOD

Details of the data analysis method are described in Appendixes A and B. An overview of the data analysis is presented below. The quality of the ER-2 measurements are discussed elsewhere: for ClO see *Brune et al.* [this issue], for N_2O see *Podolske et al.* [this issue], for H_2O see *Kelly et al.* [1989], and for ozone see *Proffitt et al.* [this issue (*a*)].

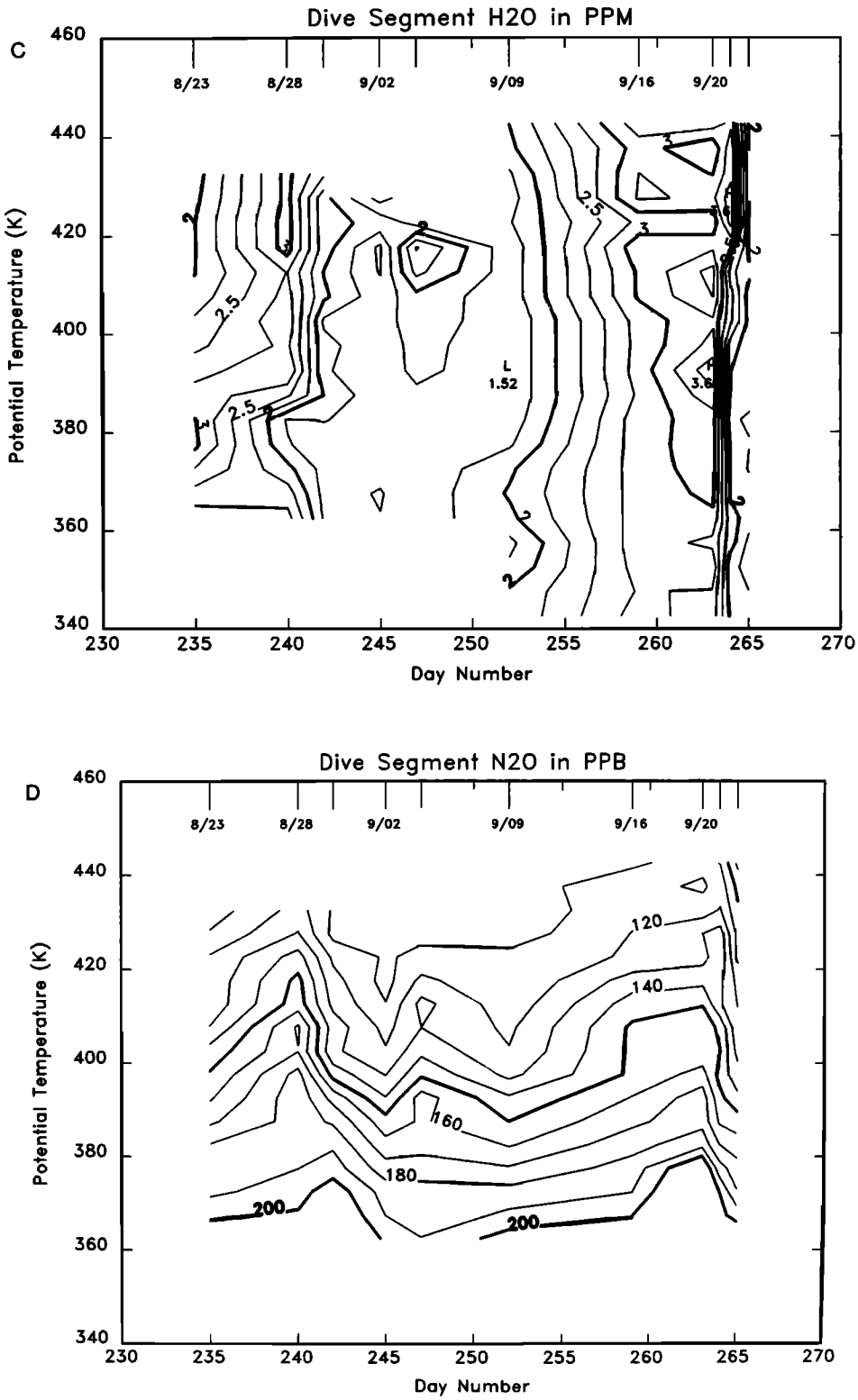

Fig. 1. (continued)

2.1. *Observations Made During the ER-2 Dives*

Observations from the dive/ascent portion of the southern end of each flight (at roughly 72°S) were averaged into 5-degree-wide PT bins. The data were then analyzed for time trends. The dive data set consists of the 10 flights after and including August 23, 1987.

2.2. *(PT, N_2O) Reference System Computations*

For each flight, the points at which a constituent was measured were located in PT and N_2O space. The flight track generally forms three sides of a roughly trapezoid-shaped envelope in (PT, N_2O) space (corresponding to the takeoff/landing, level flight, and dive/ascent portions of the

flight). Constituent values interior to the trapezoid are then estimated by linear interpolation in two dimensions within the overall envelope. The resulting constituent field in that space is sampled every 0.7 ppbv (parts per billion by volume) in N_2O and 0.68 K in PT. These daily fields were then smoothed in both directions with a boxcar average whose width was 10.4 ppbv and 10.1 K, respectively. Mean and trend analysis follows the procedure used for constituents in (PT, PV) space as described in Appendix B. The data set uses the 10 flights after and including August 23, 1989.

2.3. *(PT, PV) Computations*

The flight PV computations are described in general by *Hartmann et al.* [1989] and in Appendix A. Where PV cannot be calculated from the aircraft data (during dives, for instance), PV calculated from National Meteorological Center (NMC) global stratospheric analyses [*Newman et al.*, 1988] are interpolated to the flight path. Although the method used to compute flight PV by *Hartmann et al.* [1989] is not identical to the method described in the appendix, the results have been intercompared and show good agreement.

The NMC analyses and flight observations have also been carefully intercompared. Generally, the balanced winds computed from the NMC analysis show weaker wind gradients than flight observations. This is to be expected from the substantially lower spatial resolution of the satellite data. The difference between the NMC geostrophic winds and flight winds is −2 m/s in the mean with a 6 m/s rms deviation. The difference between the geostrophic and balanced winds is smaller than the difference between the flight winds and either NMC quantity. NMC analyses and ER-2 flight temperatures have a mean difference of 0.2 K and a rms deviation of 1.7 K. This reasonably good agreement gives us confidence in NMC PV computations over the dive and ascent portions of the aircraft flight. The data set uses the 9 flights after August 23, 1987; problems were encountered with a mismatch between flight PV and NMC PV near the dive for August 23, 1987, so that flight was not used in the (PT, PV) space analysis (see Appendix A).

3. RESULTS

3.1. *ER-2 Dives and Ascents*

Figures 1*a*–1*d* show ClO, O_3, H_2O and N_2O time series contour plots of the ER-2 observations as a function of potential temperature during the dive and ascent portions of the flights near 72°S. Dives were not made on flights prior to August 23, 1987. The long tick marks at the top of the figure indicate the dates on which the observations were taken.

Generally speaking, low-N_2O, high-ClO days represent periods when inner vortex air was sampled, as will be shown below. The sequence of days September 20–22, 1987, on the right side of the figures shows quite dramatically how the constituent concentrations at the same latitude, longitude, and potential temperature can change over a short period. Intercomparing Figures 1*a* and 1*d*, ClO and N_2O do not show large overall trends (except for the last few days, September 20–22, and near the second flight day, August 28); yet ozone (Figure 1*b*) exhibits an overall decrease above the 370-K surface. This result immediately suggests that chemical processes are controlling ozone, since the conservative tracer N_2O is nearly unchanged. Water vapor appears to show some increase during September, although the measurements indicate significant variability.

Returning to the large fluctuations in the dive data from September 20–22, Figure 2 shows the sequence of 420-K isentropic potential vorticity (IPV) maps for the last 3 days of the mission (September 20–22) and September 23. Figures 2*e*–2*h* show PV, zonal wind, and PT cross sections at 65°W for this same period. Note how the 2.5 contour of high IPV (inner vortex) air moves steadily outward toward the end of the Antarctic Peninsula in Figures 2*a*–2*d*, while the north-south gradient in IPV increases. Thus the ER-2 traveled barely into the edge of the vortex on September 20, 1987, while on September 22, 1987, it sampled inner vortex air. The constituent observations from the three dives, September 20–22, therefore represent quite dissimilar air parcel ensembles.

The PV cross sections shown in Figures 2*e*–2*h* show the downward movement of high PV contours along with equatorward movement of the polar jet from September 20 to September 23. Flight tracks on these figures show how the aircraft sampled different regions of the polar vortex.

The trend in the dive data is shown more clearly in Figures 3*a*–3*d*. A straight line has been fit to the time series shown in Figure 1 at each potential temperature level. The trend is given in the right panel, while the average and the rms deviations are shown on the left. There appears to be an increase in ClO between 380 K and 430 K of up to 0.005 ppbv/d, or about 1% per day. Note that ClO may not represent all of the active chlorine, so this trend may only indicate a change in the relative abundance of the active chlorine species such as the dimer (Cl_2O_2), OClO, etc.

N_2O in Figure 3*d* shows an increase of less than 0.5 ppbv/d or 0.25% per day below 380 K. Ozone, on the other hand, declines at a rate of 2% per day at 420 K (Figure 3*b*). As mentioned above, since N_2O shows virtually no trend in the region of significant ozone decrease, chemical processes are implicated in the ozone loss. H_2O (Figure 3*c*) appears to be increasing at a rate of about 1% per day above 400 K. We do not expect H_2O to be conservative within the CPR since air parcels may still be experiencing temperatures near the frost point as they move around the pole.

3.2. *Observations in the (PT, N_2O) Reference Frame*

Figure 4 shows ClO (Figure 4*a*), ozone (Figure 4*b*), and H_2O (Figure 4*c*) averages over the mission using PT and N_2O as coordinates. The flight path for September 22 is drawn on top of Figure 4*a* (diamonds) for reference to physical space. The number of flight days used in the generation of these figures are shown in Figures 4*d*–4*f*. Only flights after August 23, 1987, were used; previous flights had no dives. Time series analysis was performed only when data at the same point in (PT, N_2O) space could be obtained from three or more flights.

The upper left edge of Figures 4–6, corresponding to high PT and low N_2O, is the region inside the polar vortex at highest aircraft altitudes. A line from the upper left edge moving toward the lower right edge marks the high-ClO domain and roughly locates the dive zones inside the vortex. This region also corresponds to the domain of relatively lower ozone and low water vapor. The top right and center of the figure represent the upper altitude region outside the polar vortex. Ozone values are 2–3 ppmv (parts per million

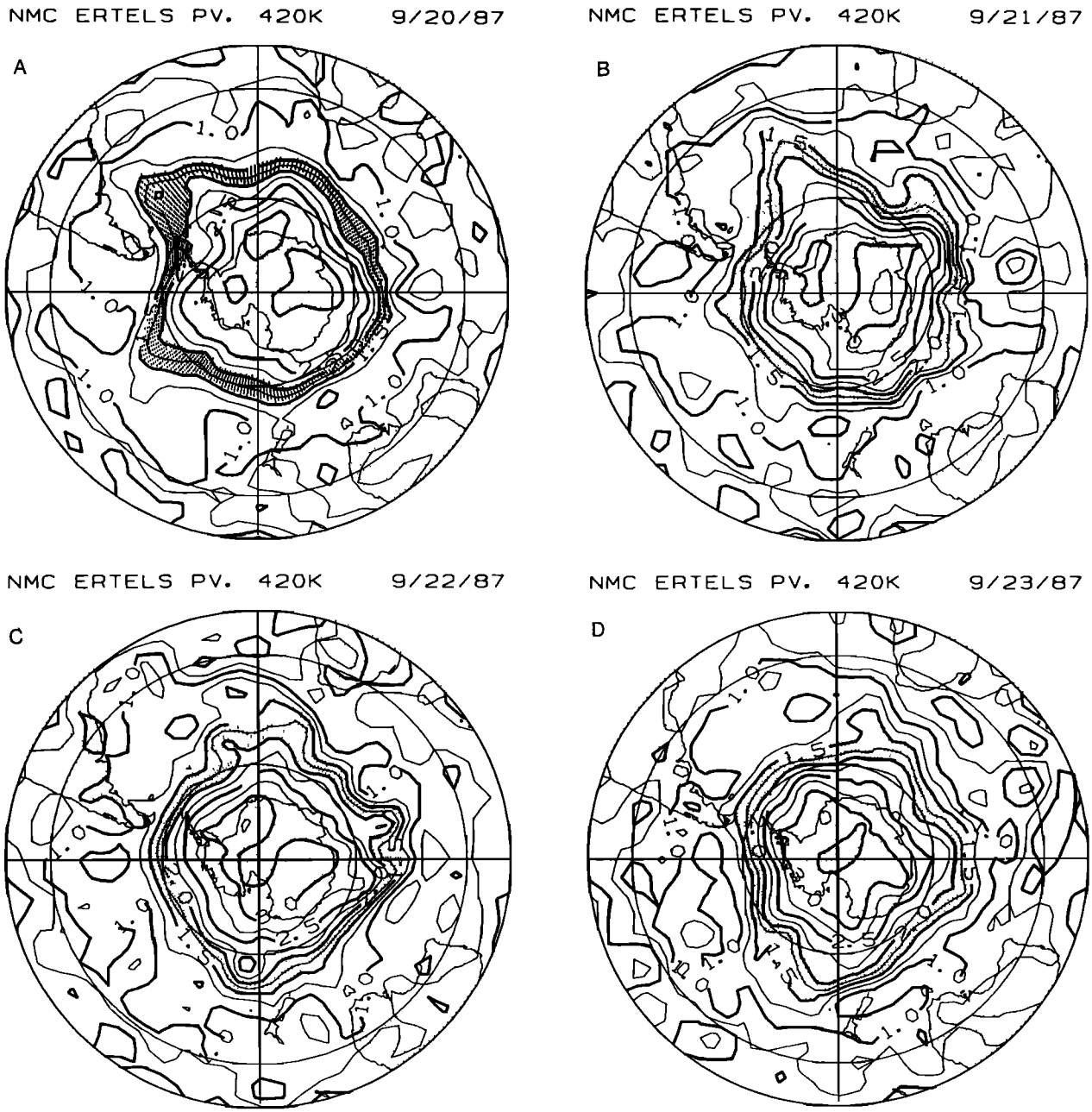

Fig. 2. Potential vorticity on the 420-K potential temperature surface: (*a*)–(*d*) September 20–23, 1987, respectively. Polar stereographic maps after *Newman et al.* [1988] except that balanced winds are used in the computation. The outer circle corresponds to 20°S with other circles at 30°S and 60°S. A PV value of 1 is $-1.0e - 5$ K m/s^3/Pa. Shading is between 1.5 and 2 units. (*e*)–(*h*) Cross sections of the NMC analysis at 65°W corresponding to the maps shown in Figure 2; PV values are displayed as heavy solid lines. In Figures 2*e*–2*h*, thinner solid lines show the zonal winds in 5 m/s intervals while dashed lines show potential temperature in 20-K increments. The thinnest solid lines on the September 20–22 plots indicate the flight path of the ER-2. The left axis is the log-pressure altitude, 7 km × $\log_e$ (1000/*p*), where *p* is pressure in millibar; the right axis gives pressure.

by volume) or higher in that region; ClO values are below 0.1 ppbv, and H_2O is 4 ppmv. As previously mentioned, ClO is not the only reservoir for active chlorine, but since most flights are made into the CPR near local noon, we assume that the dimer Cl_2O_2 is photolyzed so that ClO measurements probably reflect a significant fraction of the active chlorine.

The most interesting feature of Figures 4*a* and 4*b* is the collocation of the minimum in ozone and maximum ClO along the lower left edge of the figure. However, unlike H_2O, which decreases continuously toward the lower left edge of the envelope, ozone shows a decrease then increases slightly. Thus the ozone minimum appears to have an annular structure with the lowest values not at the inner edge of the sampled CPR but equatorward of it.

Figure 5 shows the trends in ClO, ozone, and H_2O corresponding to the data shown in Figure 4. It is evident from Figure 5*a* that little trend in ClO is evident in the high-ClO region (see Figure 4*a*) except near the lower left edges of the figure (dive region). The trend at the lower left

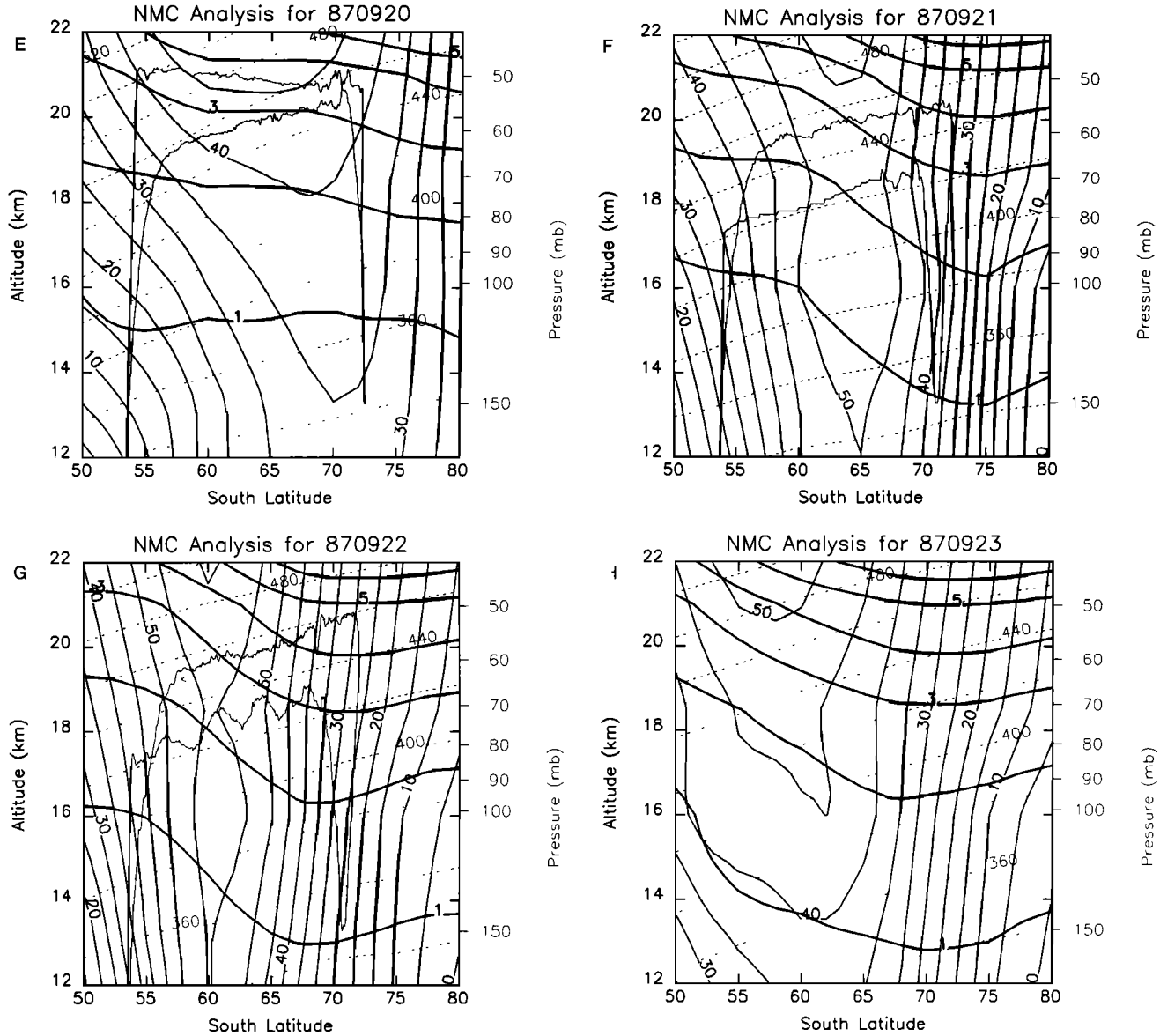

Fig. 2. (continued)

appears at deepest penetration of the vortex and suggests that ClO formation is still taking place during the mission, although the trend is less than half that obtained from the dive data (Figure 3*a*). Since the dive data are composited irrespective of the extent of the aircraft penetration into the vortex, the dive data trend in ClO is probably more uncertain. Trends in ClO at the far right and far left of Figure 5*a* are based upon too few data points to be certain.

Figure 5*b* shows a significant decrease in ozone over a broad region corresponding to the high ClO zone in Figure 4*a*. The decrease rate is generally about 0.04–0.06 ppmv/d, again in agreement with the dive data shown in Figure 3*b*. Since this decrease takes place with air parcels having the same potential temperature and N_2O, the decline must be chemical in origin. The trends in water vapor within the CPR (Figure 5*c*) are also consistent with the dive data (Figure 3*c*); the increase is about 0.03 ppmv/d.

Outside the CPR as defined by high ClO in Figure 4*a*, both ozone and H_2O show a slight increase (Figure 5*c*). *Proffitt et al.* [1989] argues that this increase is due to diabatic descent of air outside the vortex. Since both water vapor and ozone increase with potential temperature outside the CPR, this conclusion seems reasonable. The ozone change is about 0.02 ppmv/d outside the CPR. Using Figure 4*b*, for example, the vertical gradient in ozone is about 0.032 ppmv/K (potential temperature) in the region with the greatest trend outside the CPR giving a potential temperature change of −0.64 K/d or a cooling rate of 0.3–0.4 K/d (e.g., $H = d\theta/dt \simeq (dO_3/dt)/(\partial O_3/\partial\theta)$). A similar computation performed for water gives 0.75 K/d with much more uncertainty because of the weaker vertical gradient in water vapor. Note that the largest trend in water vapor occurs where the gradient in the PT direction in Figure 4*c* is weak. These cooling rates outside the CPR are somewhat smaller but not inconsistent with those estimated by *Proffitt et al.* [this issue (*b*)]. They are in reasonable agreement with the radiative transfer calculations of *Rosenfield et al.* [1987] for July at this latitude.

Figures 6*a*–6*c* show the rms deviation of daily constituent

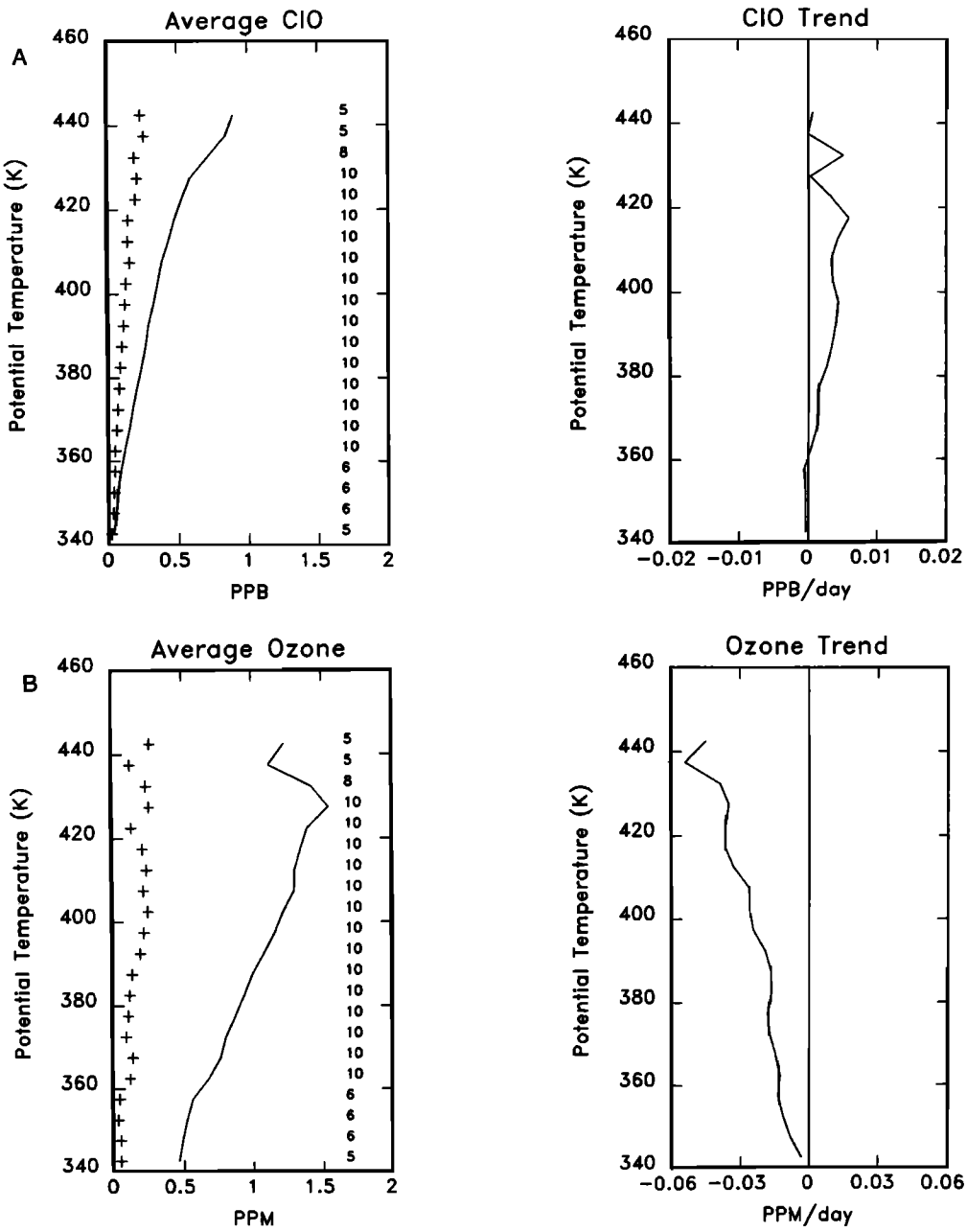

Fig. 3. Trends, average values, and rms deviation of the dive data after the trend is removed for (*a*) ClO, (*b*) ozone, (*c*) H_2O, and (*d*) N_2O. The number of days used to assess the trend is given on the right side of the left panel; the rms deviations are shown as pluses, the average value is the solid line; for N_2O the rms deviation is increased by 100 ppbv so that the same axis can be used.

fields from their linear fits in time (Figures 4 and 5). The ozone rms deviation in the region where at least 10 flights within the vortex are used is generally less than 0.15 ppmv, compared to 0.23 ppmv from the dive data (Figure 3). A similar reduction in the rms deviation in the ClO measurements in the dive region is also evident. This reduction of the variance increases our confidence in the trends. Where fewer points are available, at the edges of the region, larger rms deviations are evident.

One unusual feature of Figure 6*a* is the larger variance in ClO at the edge of the CPR. This region roughly locates a broader zone extending upward and downward along the edge of the high-ClO regime. A similar pattern is seen in Figure 6*c* where a high rms deviation in H_2O is located at the edge of the CPR. Moving poleward from the tip of South America, N_2O changes smoothly on a potential temperature surface relative to H_2O, ClO, and (toward the end of the mission) ozone [*Proffitt et al.*, 1989; *Anderson et al.*, 1989]. The abrupt change in the constituents has been used by *Proffitt et al.* [1989] to define the edge of the CPR. Since N_2O is chemically neutral at these altitudes and changes slowly crossing into the CPR, air parcels with similar values of N_2O can have quite dramatically different chemical compositions at the CPR edge. Thus any uncertainty in N_2O resulting from observational error or numerical processing will produce a larger degree of variability in species like ClO in the (PT,

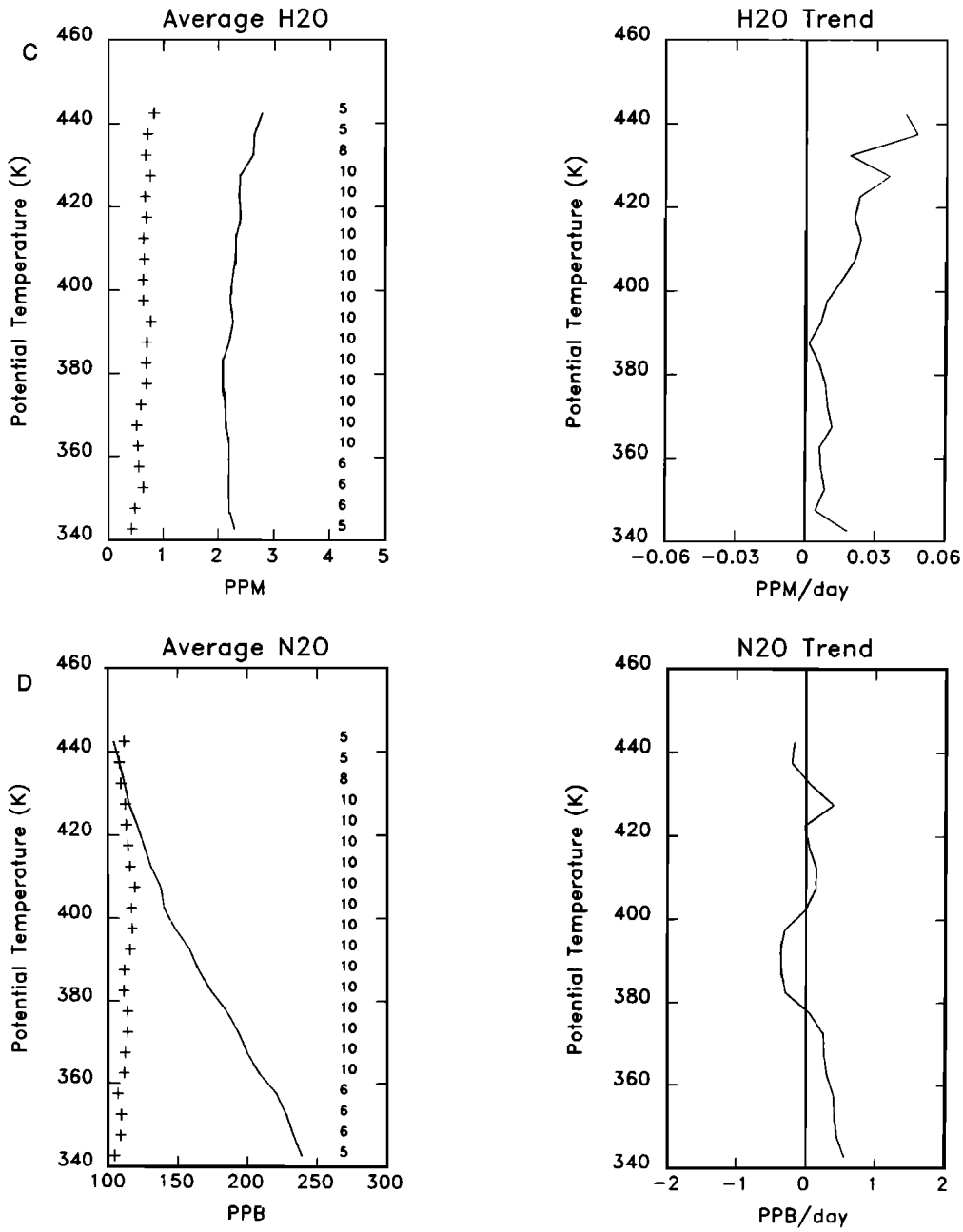

Fig. 3. (continued)

N_2O) reference frame. The net result is a zone of high variance in ClO near the edge of the CPR. In general, any constituent which has a high degree of spatial variability relative to the conservative coordinate frame (such as N_2O and PT) may not show a significant reduction of variance in the conservative coordinates relative to physical space, and, in fact, the variance may increase.

3.3. *Observations in the (PT, PV) Reference Frame*

Observations in the (PT, PV) reference frame are constructed as discussed in section 2.3 and in Appendix B. Figures 2*e*–2*g* show PV, PT, and zonal wind contours using NMC data for September 20–22, flight days which typify the range of stratospheric meteorological conditions that prevailed during the mission. Near the pole, where the PT and PV contours tend to be nearly parallel to each other, the coordinates become degenerate.

Figure 7 shows the flight track of the aircraft in (PT, PV) space for September 22, 1987, along with ozone computed by bilinear interpolation from flight measurements onto the (PT, PV) grid for that day. As with the (PT, N_2O) plots, the dive portion of the flight is along the lower left edge of the shaded region.

The mean values for ClO, O_3, H_2O, and N_2O in (PT, PV) space are shown in Figures 8*a*–8*d*, respectively. The number of flight data points used in generating these figures is not shown, but the pattern is similar to that shown in Figures 4*d*–4*f*, with the exception that data from August 23, 1987 is not used.

Referring first to Figure 8*d*, the general vertical alignment

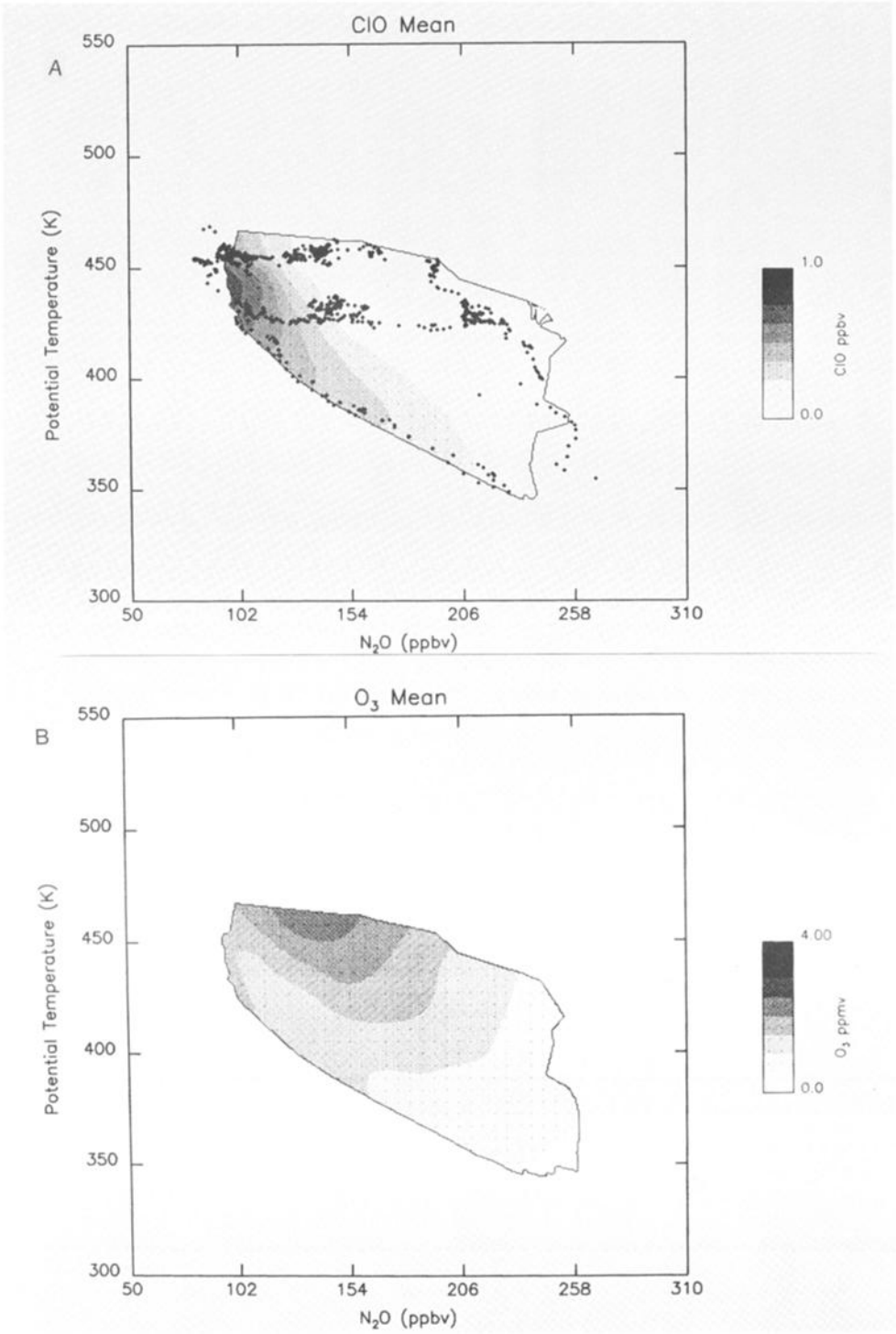

Fig. 4. Averages of (*a*) ClO, (*b*) ozone, and (*c*) H_2O in potential temperature–N_2O space. This plot is constructed from all ER-2 flights with dives (data after and including August 23, 1987). A thin line encloses the envelope containing data obtained from more than three observations. The diamonds on Figure 4*a* indicate that N_2O sample points for September 22, 1987; takeoff is on the right side with the dive indicated by the line of points on the lower left. The aircraft flies out to the most southerly point on one PT surface, returning on another. (*d*)–(*f*) The number of days used in the composites.

of the contours of N_2O show that this constituent is principally a function of PV, despite the strong vertical stratification of all three quantities. This suggests that the N_2O and PV distribution are closely tied together. In other words, the major mixing processes in this part of the stratosphere involve adiabatic motion, and each parcel retains memory of its PV and N_2O value. Figure 8*d* also shows that N_2O and PV are nearly degenerate conservative coordinates, since the PV and N_2O values have roughly the same absolute gradient along any PT surface. Thus a (PV, N_2O) coordinate system would not be helpful in reducing rms deviation. Despite their similarities, there are weak variations in the

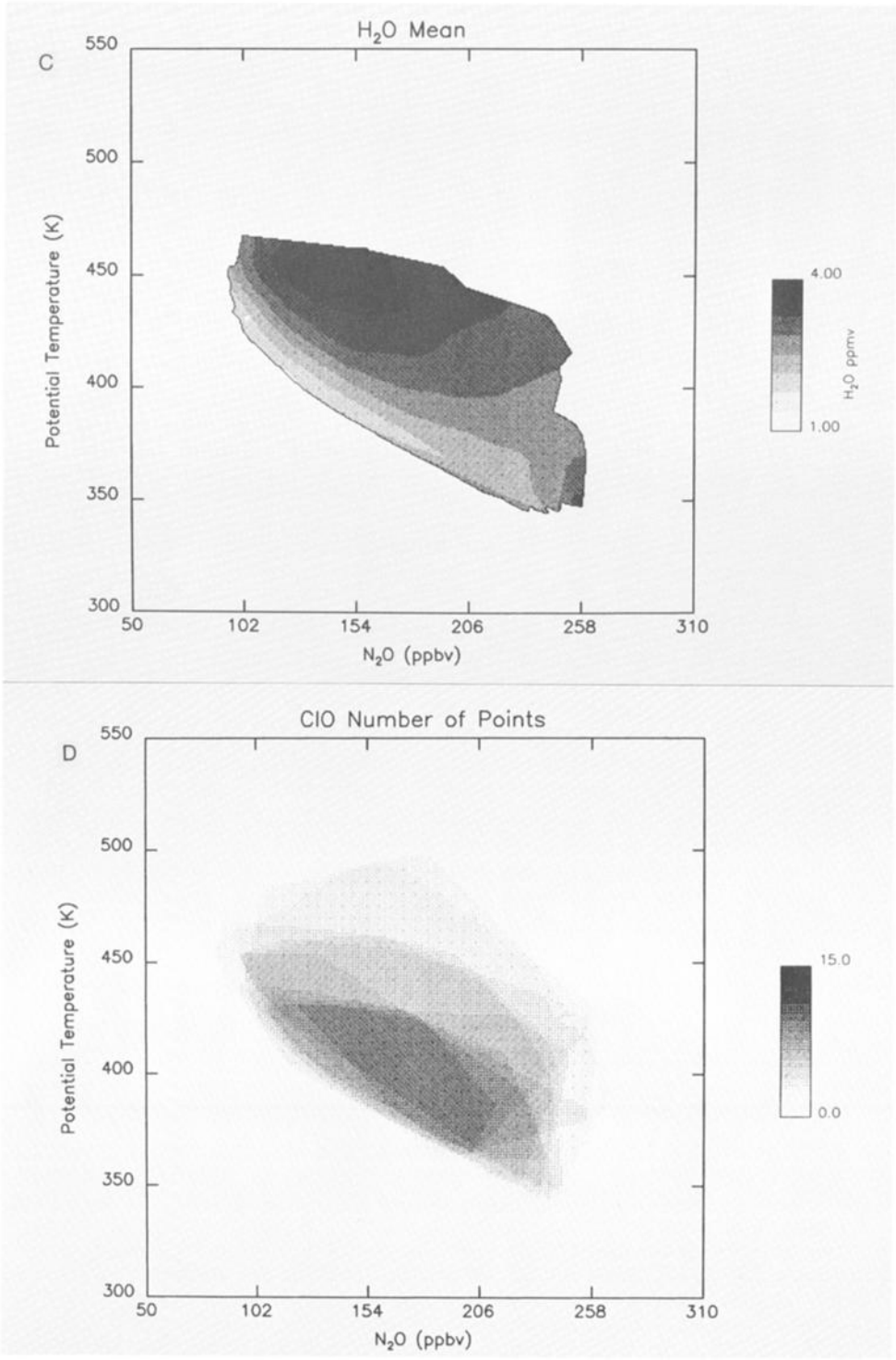

Fig. 4. (continued)

N_2O field with PT which indicates that there are important differences in the relative gradients of the two quantities. This is not unexpected, since the response of the potential temperature and N_2O field to the seasonal change in the diabatic forcing will be different.

Figure 8*a* shows the ClO composite in (PV, PT) space; the region of high ClO delineates the CPR. This figure should be compared to Figure 4*a*, the composite in (N_2O, PT) space. The two figures are in general agreement as expected from the similarity between N_2O and PV. Figure 8*b* shows the ozone field in (PT, PV) space. Again, the general structure is similar to that in Figure 4*b*; the depletion region appears at the lower left side of the figure, although not as strikingly evident as in Figure 4*b*. The annular structure noted in Figure 4*b* is also evident. The mean H_2O field also resembles Figure 4*c*.

Figures 9*a*–9*d* show the trend in the (PT, PV) reference frame for the quantities shown in Figure 8. Figure 9*d* shows that N_2O has virtually no overall systematic trend greater than 1 ppbv/d within the CPR region. This translates into a

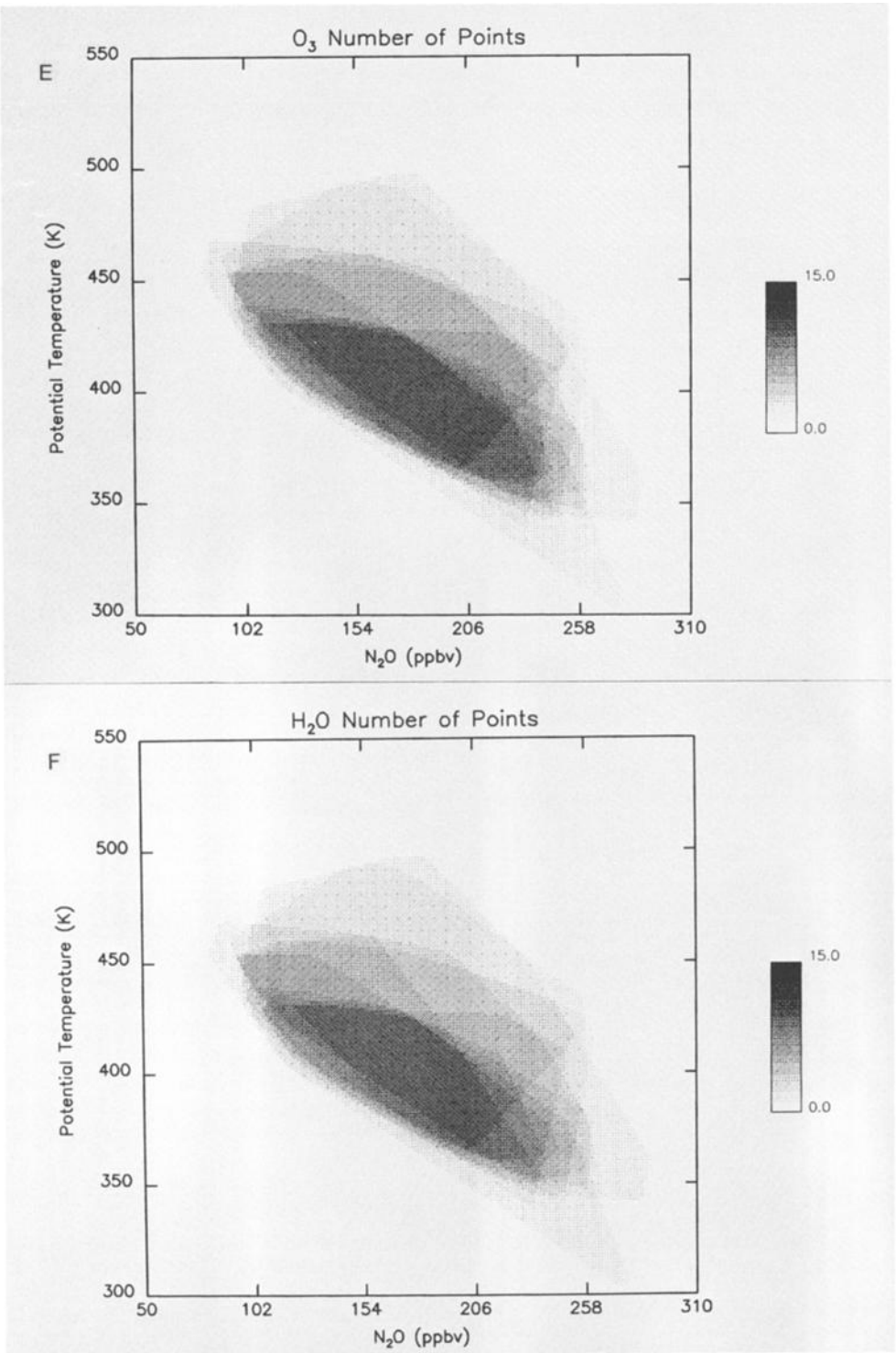

Fig. 4. (continued)

cooling rate of less than 0.2 K/d, consistent with the analysis of *Hartmann et al.* [this issue]. Outside the CPR in the middle stratosphere (430, $-2.5E-5$) (read $-2.5E-5$ as -2.5×10^{-5}), N_2O shows an increase of about 2 ppbv/d.

Ozone shows a significant decrease in the CPR region at a rate similar to that shown in Figure 5*b*. An increase in ozone near (450, $-2.7E-5$) is also evident; this is in the same region as the increase noted in Figure 5*b*, although the trend is slightly larger. In the region corresponding to the increase in N_2O at (430, $-2.E-5$), a slight decrease in ozone is evident. Since the vertical gradients of the two constituents are opposite, the trend in this region is consistent. On the other hand, N_2O is slightly increasing in the region (450, $-2.7E-5$), where ozone is increasing. The rms deviations, shown in Figure 10, are not large in these regions so the trends may be significant. These features result from the variation of the ozone and N_2O gradients with respect to each other. Whereas N_2O decreases steadily along the PT surface moving toward the CPR from subpolar latitudes, ozone shows a more complex variation (Figures 8*b* and 8*d*).

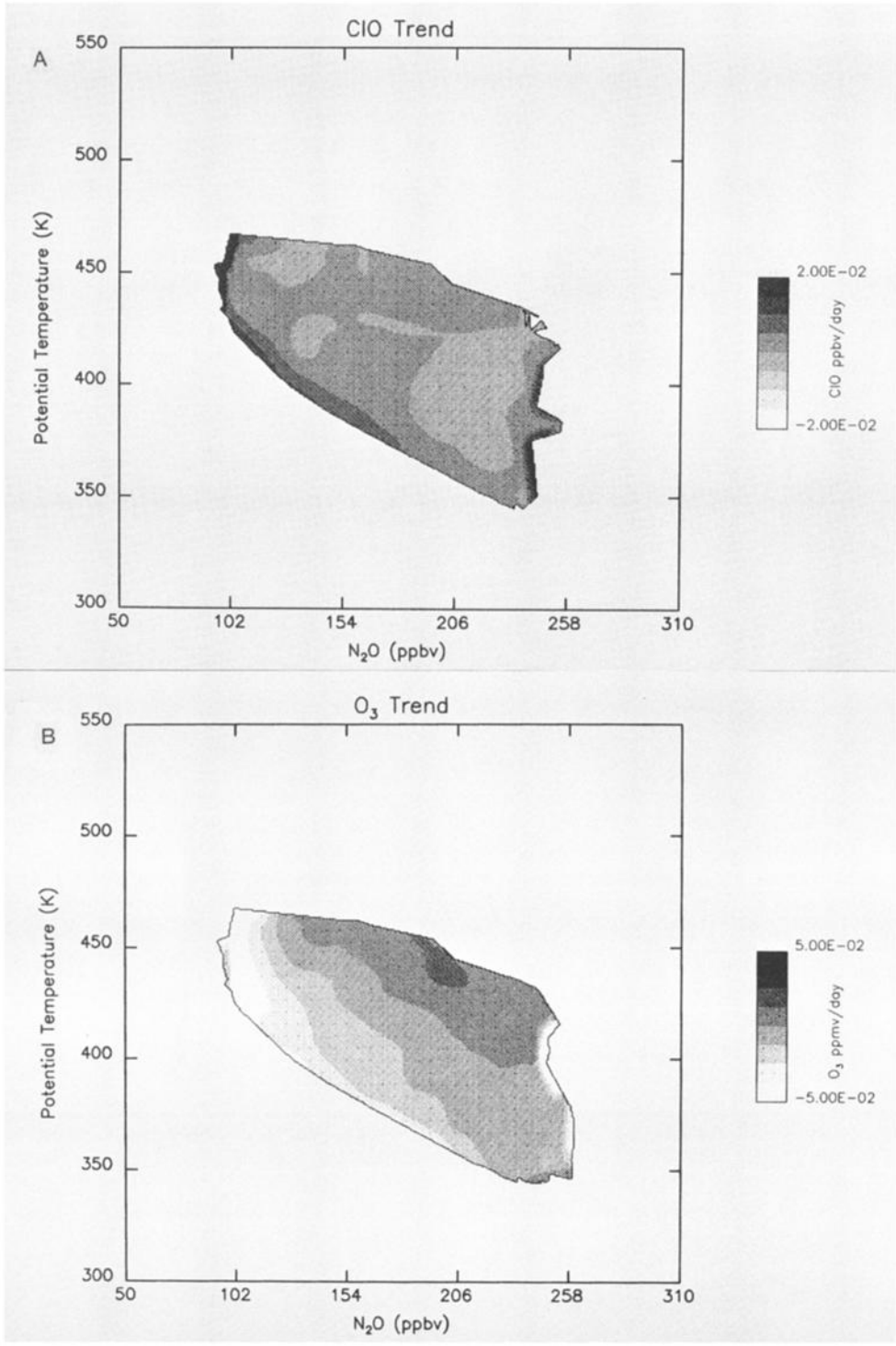

Fig. 5. Same as in Figures 4*a*–4*c* for the trends in ClO, O_3, and H_2O. Flight track is not shown.

In the region (430, $-2.E-5$), ozone and N_2O are vertically stratified in (PT, PV) space, but their gradients are reversed. Weak diabatic heating would produce an increase in N_2O and an ozone decrease in that region. From Figures 8*b* and 9*b* we estimate this heating to be less than 0.6 K/d. The physical space location of this region can be identified using Figures 2*e*–2*h*.

In the (450, $-2.7E-5$) region, ozone and N_2O gradients tend to be more aligned so trends driven by diabatic motion will have the same sign. We estimate the cooling in this region to be about 0.5 K/d from N_2O and 0.6 K/d from O_3. These values are in reasonable agreement with the cooling rates computed for the same region using (PT, N_2O) space. Note that the computations of the heating rates presume that the PV field is fixed; if body forces act on the flow or if there is a strong vertical gradient in the heating, then changes in the PV field may give rise to spurious trends in the constituents.

The ClO and H_2O trends shown in Figures 9*a* and 9*c* generally agree with the corresponding Figures 5 and 3.

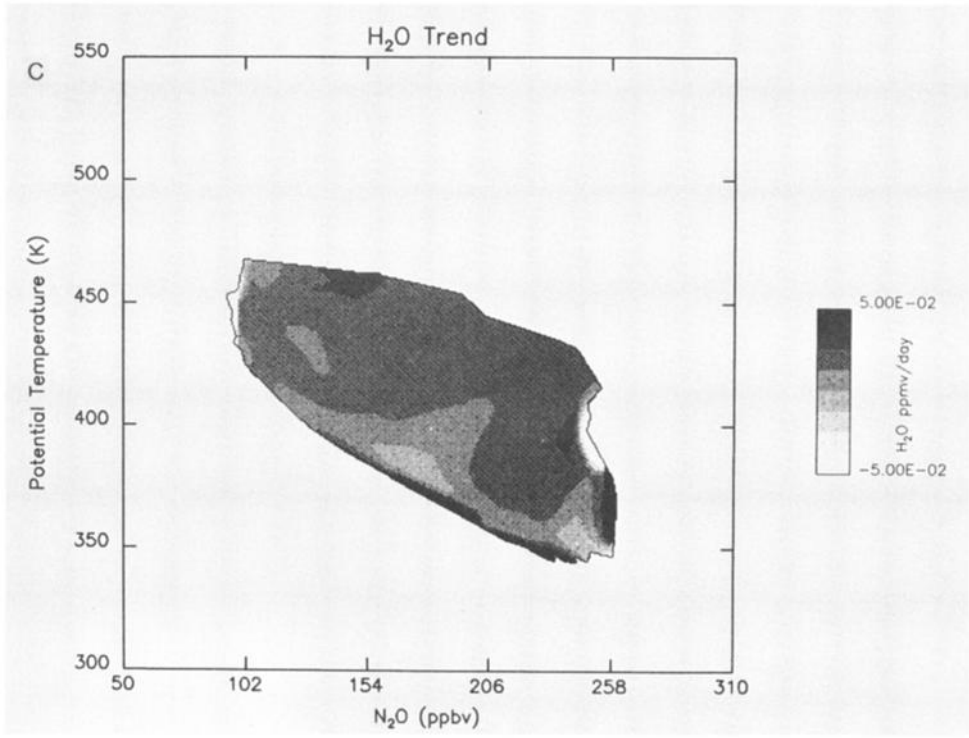

Fig. 5. (continued)

Outside the CPR, H_2O shows some increase in both N_2O and PV coordinate systems. However, ClO shows a decrease outside the CPR at (450, $-3.5E-5$). This decrease is located in a region of high variance and may be discounted (Figure 10*a*). H_2O also shows an anomalous decrease at the top edge of the envelope in Figure 9*c*; no such trend is evident in Figure 5*c*, even though the variance is small. The decrease in H_2O in this region is therefore suspect. At this point it is clear that composites in (PT, N_2O) and (PT, PV) are supplementary calculations in the sense that trends can be verified only when they appear in both coordinate systems.

Comparing the rms deviations in Figures 10*a*–10*c* with Figures 6*a*–6*c*, the overall results appear to be similar. Although the variance for ozone is slightly higher than that computed in (PT, N_2O) space, it is still substantially reduced

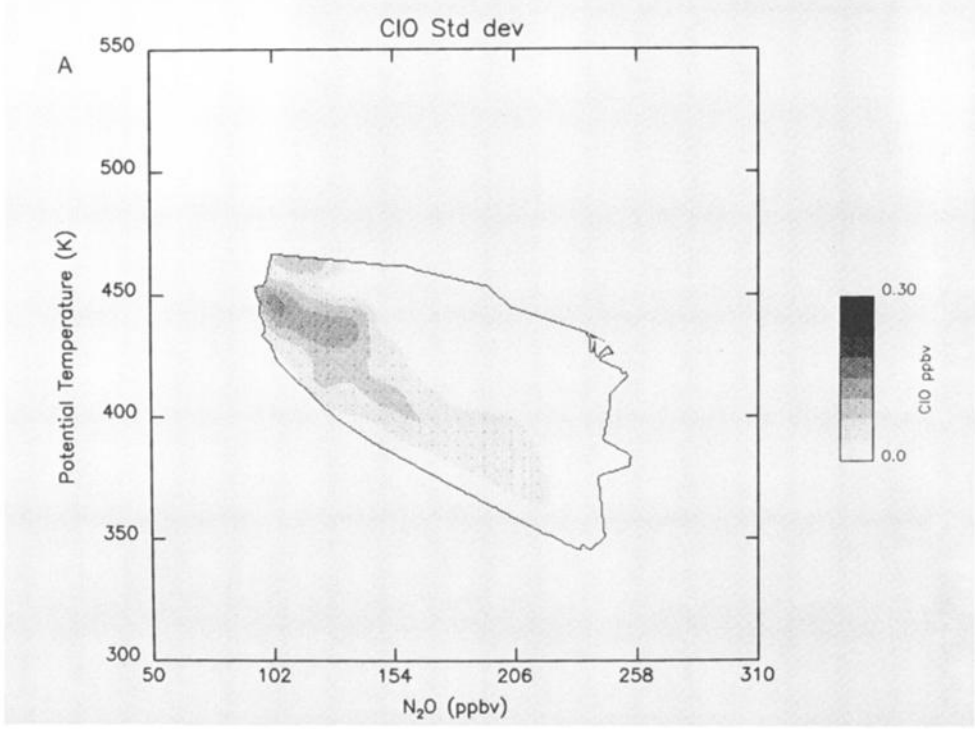

Fig. 6. The rms deviation in time from the trend for the composites shown in Figure 4*a*–4*c*.

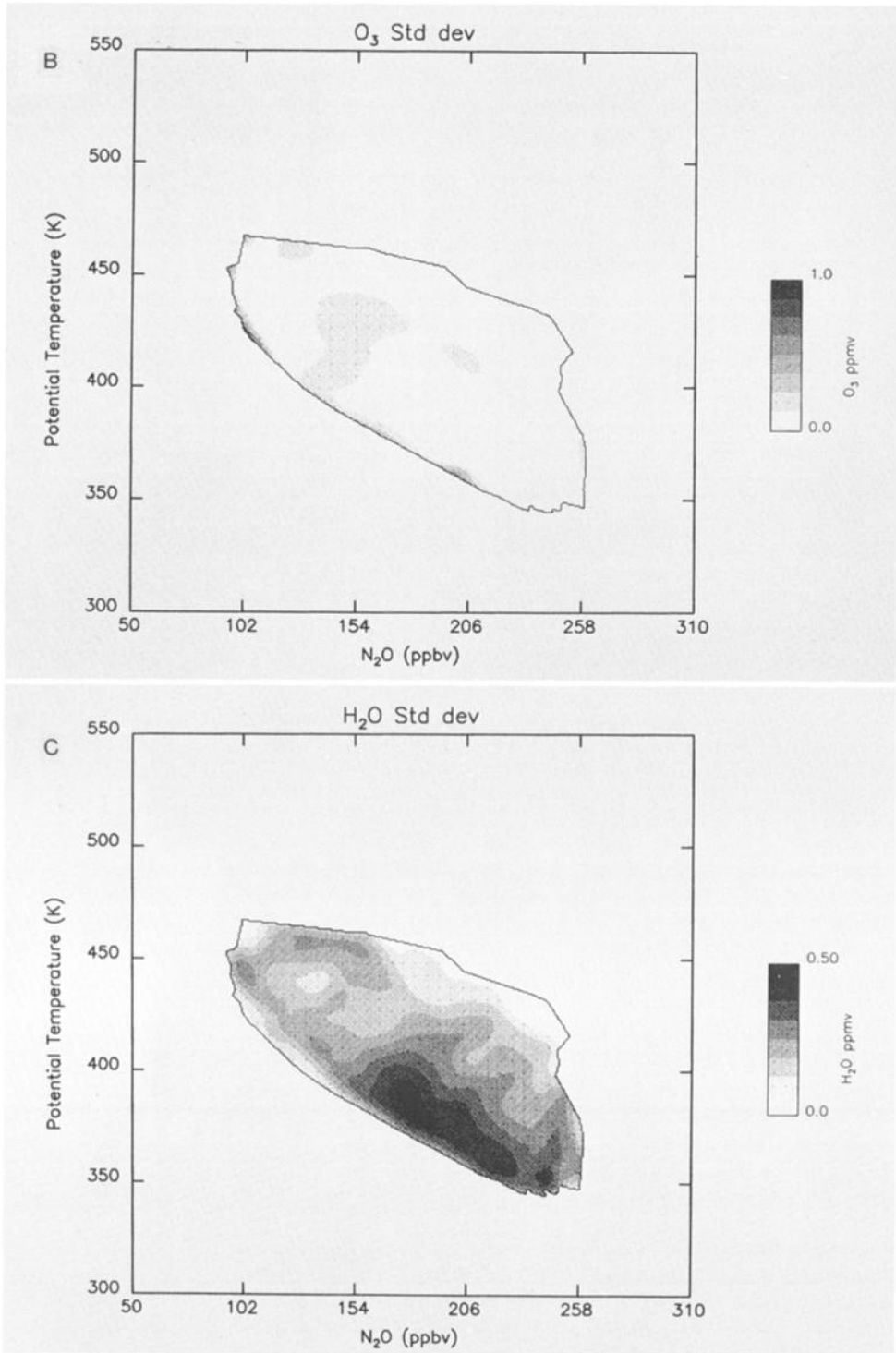

Fig. 6. (continued)

in the CPR, compared to the dive observations. The pocket of high ClO variance at the edge of the CPR is similar to that shown in Figure 6*a* and is due to the large gradient in ClO along the coordinate surfaces. N_2O shows large variance in the low (PT, PV) regions (right side of figure), where NMC PV values are used. This variance may be a reflection of the quality of the lower-altitude meteorological data.

To summarize, the (PT, PV) transforms and (PT, N_2O) transforms both show similar overall results: (1) that ozone is decreasing within the CPR in a conservative coordinate system and that this decrease therefore is chemical in nature; (2) ozone is increasing outside the CPR in the 18–20-km region at a rate which corresponds to a diabatic cooling rate between 0.3 and 0.6 K/d (There is some evidence for weak diabatic heating at lower latitudes.); (3) ClO is increasing within the CPR; and (4) N_2O and PV are roughly equivalent conservative coordinates.

3.4. *Physical Space Reconstructions*

The (PT, PV) space observations and trends can be inverse transformed back to physical space to view the

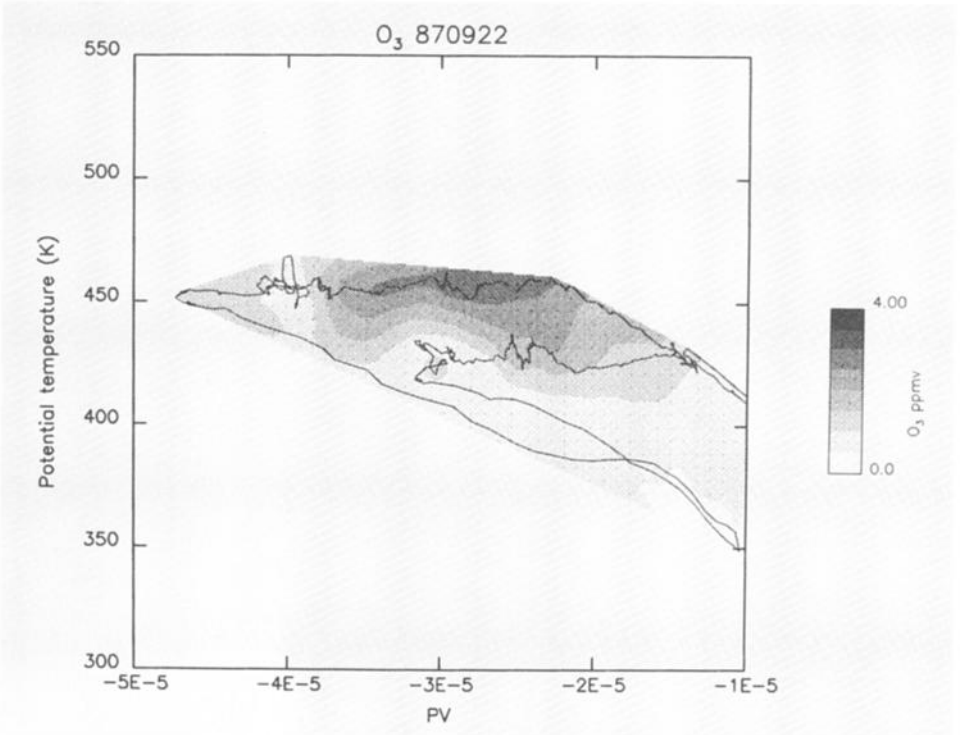

Fig. 7. Ozone interpolated into (PT, PV) space for September 22, 1987, and the corresponding flight path. As with Figure 4*a*, aircraft takeoff is on the right and dive on the lower left.

overall structure of the constituent fields. This transformation reconstructs the fields in the region outside the aircraft flight area. The method is described in Appendix B. Reconstructions for the last 3 days of the mission will be presented and compared to flight observations in this section. In addition, the projected constituent values are used to reconstruct the fields for September 23, 1987, although no flight data are available on that date for verification. These 4 days generally represent a period when inner vortex air moves in along the Antarctic Peninsula with ClO increasing and N_2O decreasing along the southern portion of the flight track.

September 20, 1987. Figure 11 shows the reconstruction for September 20, 1987, of ClO, O_3, H_2O, and N_2O, respectively, the original data, PV, PT, and the flight track for September 20, 1987. More of the meteorological fields are shown in Figure 2.

The agreement between the reconstructions and the observations is generally quite good. Recall that the inverse transform for the reconstructions is applied to the constituent fields calculated from the means and trends. Furthermore, flight data are used in the transform to (PT, PV) space, while only NMC data are used in the inverse transform. Differences between the observations and the reconstructed fields along the flight track therefore are to be expected.

In general, the reconstructions give an accurate and physically simple picture of the polar vortex structure. N_2O (Figure 11*d*) shows a downward displacement within the CPR, which itself is well defined by high ClO (Figure 11*a*) and low H_2O (Figure 11*c*). Reconstructed ozone (Figure 11*b*) shows a tongue extending downward and equatorward of the CPR, roughly at the location of the jet core (Figure 2*e*). This tongue is not simply the remnant of a broader downward displacement of the ozone layer modified by ozone destruction inside the CPR, since the tongue is also evident in the reconstructions generated for August. The ozone tongue also shows up as the peak in ozone near (450, 140 ppbv) in Figure 4*b* and (450, $-2.8E-5$) in Figure 8*b*. The tongue appears to be roughly coincident with the region of descending air outside the CPR, suggesting that most downward transport is taking place just outside the CPR.

The decrease in ozone within the CPR is also evident in Figure 11*b*. From Figure 2, it is apparent that the flight of September 20, 1987, barely penetrated the CPR; this is also clear from the reconstructions of ClO (Figure 11*a*), which show higher ClO levels poleward of the aircraft dive. Note that the CPR edge in ClO is smoothed out by reconstruction, with high ClO beginning at 68°S in the flight data (Figure 11*a*, left) but beginning at 66°S (right) in the reconstruction. Within the CPR the highest values of reconstructed ClO appear poleward of the aircraft-measured values. This type of discrepancy is not unexpected where a sharp constituent gradient exists relative to the PV field. Recall that the transformations into (PT, PV) coordinates involve boxcar smoothing, and the inverse transformations use only the lower-resolution NMC data.

In the dive regions the reconstruction tends to overestimate the constituent mixing ratio for O_3 and N_2O. The ozone depletion region within the CPR is placed too far south.

September 21, 1987. Figure 12 shows the results for September 21, 1987. Comparing Figures 11*d* and 12*d*, low N_2O values have pushed northward and downward from the pole. Figure 2 shows that the PV gradients have tightened along the Antarctic Peninsula, the jet has strengthened, and inner vortex, high PV air has moved closer to the tip of South America. The ozone distribution shows similar changes. The aircraft penetrated further into the CPR on this date; note the increased ClO and ozone gradients on the CPR

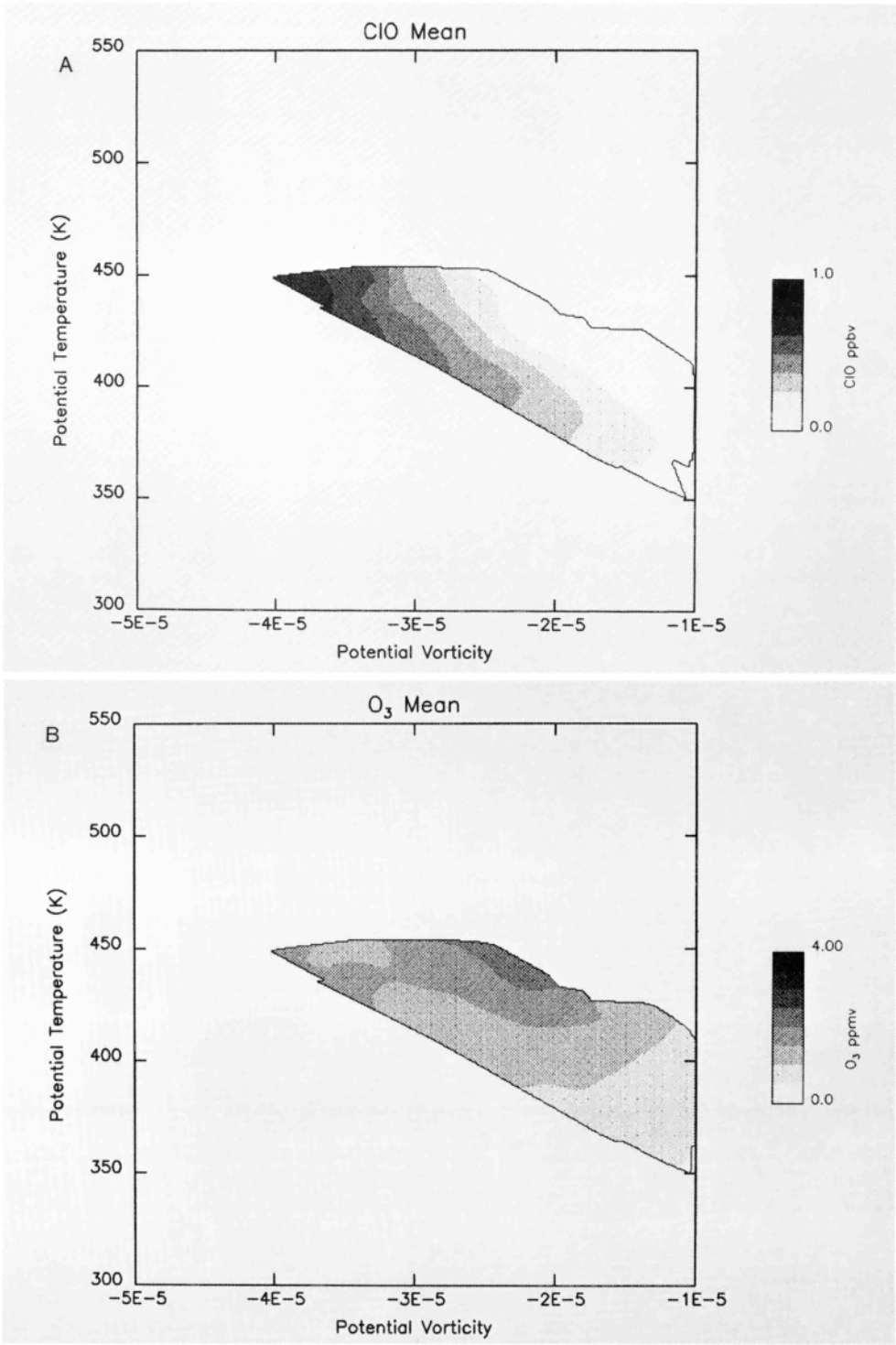

Fig. 8. Averages of (*a*) ClO, (*b*) O_3, (*c*) H_2O, and (*d*) N_2O in (PT, PV) space. This plot is constructed by averaging the nine ER-2 flights after August 28, 1987. A thin line encloses the region with at least three observations.

edge. The reconstructed ClO and ozone gradients are comparatively smoothed.

September 22, 1987. Figure 13 shows the results for September 22, 1987. Inner vortex air moves even closer to Punta Arenas in comparison to September 20, 1987, and the jet intensifies. Note the apparent downward movement of the N_2O field in Figure 13*d* compared to Figure 12*d*. Low N_2O values also move further north along the flight track, but below 18 km the horizontal N_2O gradient reverses, suggesting a fold in the PV field. This interpretation is consistent with Figure 2*c*, which shows a tongue of high PV air extending westward along the Antarctic Peninsula and a fold in PV at the base of the peninsula.

Figure 13*b* shows that low-ozone, low-H_2O CPR air has moved to lower latitudes; and high-ozone, high-H_2O air is still collocated with the jet core (Figure 2*g*). Again, in comparison to the observations, the reconstructions tend to wash out the sharper gradients. An unusual feature is the

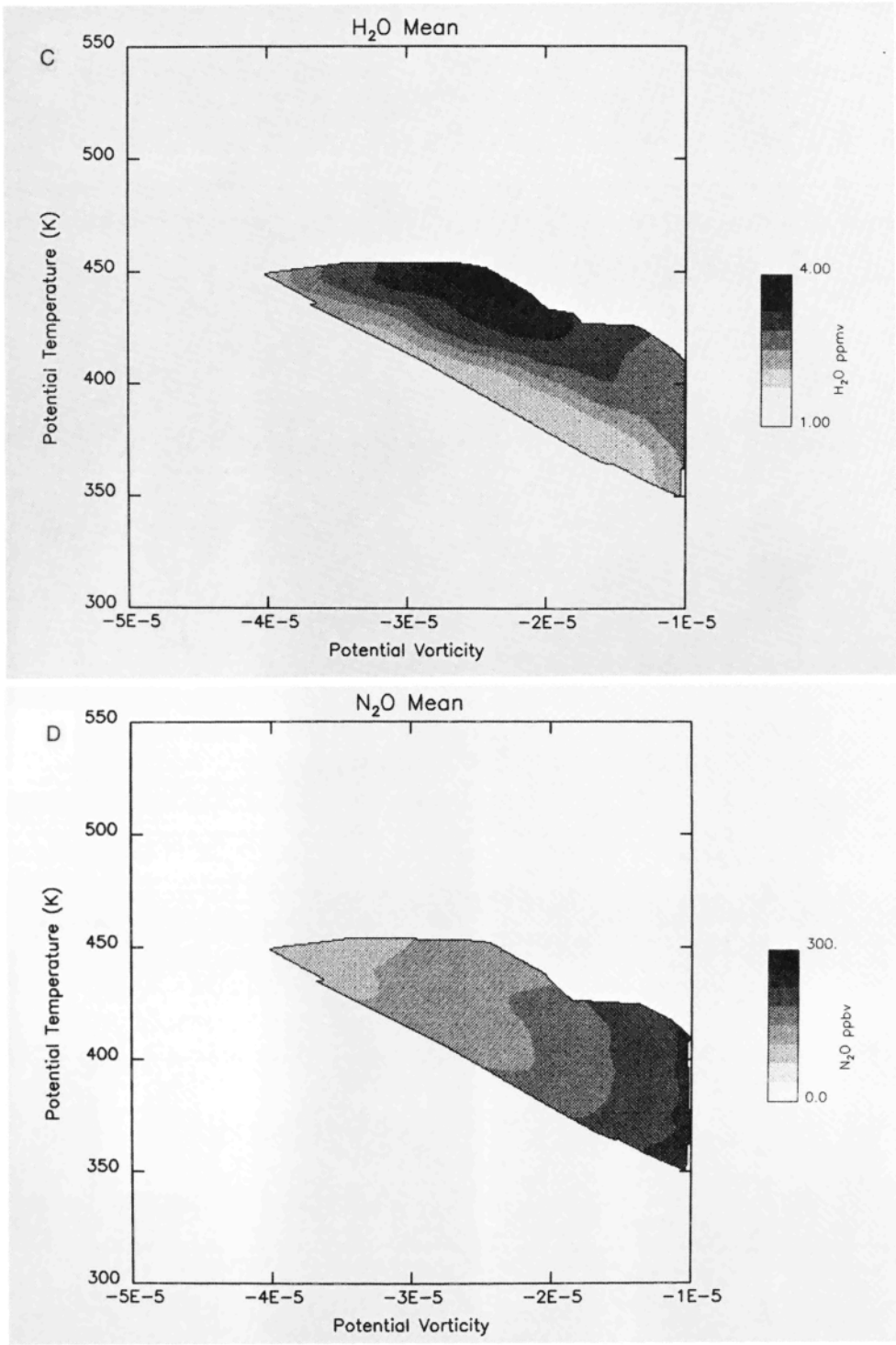

Fig. 8. (continued)

increase in ozone in the flight observations poleward of 70°S; this feature also appears in the reconstruction when more shading intervals are used. The appearance of this inner CPR increase in ozone is consistent with the NMC picture of an extrusion of the vortex extending across the peninsula (see Figure 2*c*). Figure 13*a* shows that the highest levels of ClO have also moved downward along the flight track, consistent with the N_2O and O_3 changes.

September 23, 1987. Although no flights occurred on this day, reconstructions can still be performed using the constituent fields reconstructed from the linear time fit, along with the NMC PV and PT fields. The results, shown in Figure 14, indicate a continuation of the tendencies of the previous days. High PV and ClO values move to lower altitudes and push to lower latitudes; low N_2O values follow the same pattern. However, although the jet is still in roughly the same position, it has weakened (Figure 2*h*), and the PV gradients are weaker across the Antarctic Peninsula.

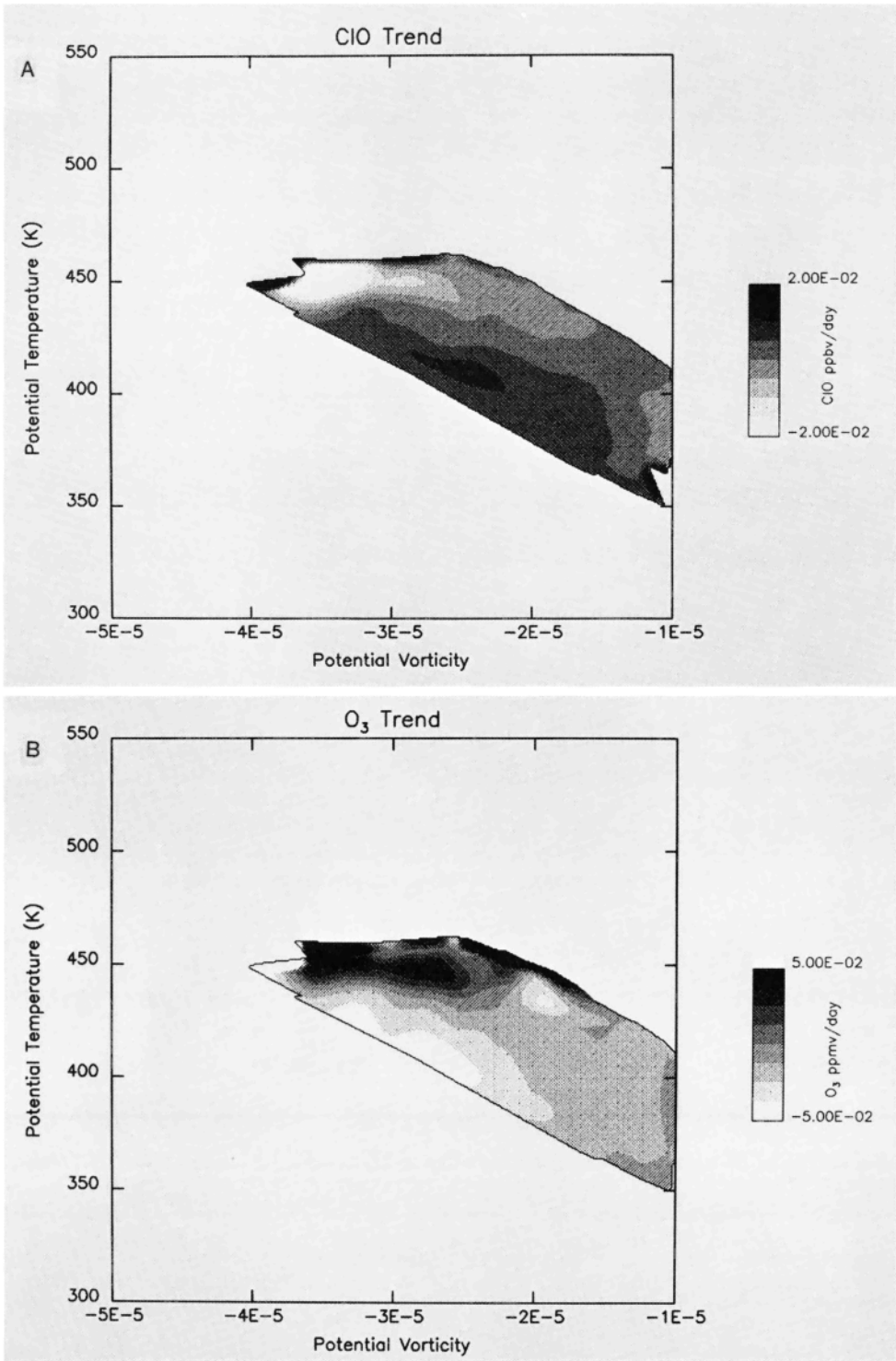

Fig. 9. Trends computed from constituent observations shown in Figure 8.

As expected, the reconstructions show weaker constituent gradients.

4. Summary and Conclusions

Using conservative reference frames constructed from PT, N_2O, and PV, ER-2 constituent measurements of ClO, H_2O, and ozone have been analyzed. The coordinate transformation to the conservative reference frames is similar to the Modified Lagrangian Mean method proposed by *McIntyre* [1980] and allows for changes in species to be interpreted without the complications associated with the motion of the vortex. Poleward of the jet core, this procedure generally reduces the rms deviation of the measurements by about one-half compared to the deviations in physical space. The variance does not vanish, however, because (1) the gradients of PT, N_2O, and PV are not as large as some of the nonconserved species, so that numerical uncertainty exists in their assignment in the conserved coordinates; and (2) there may be natural zonal variance in chemically active

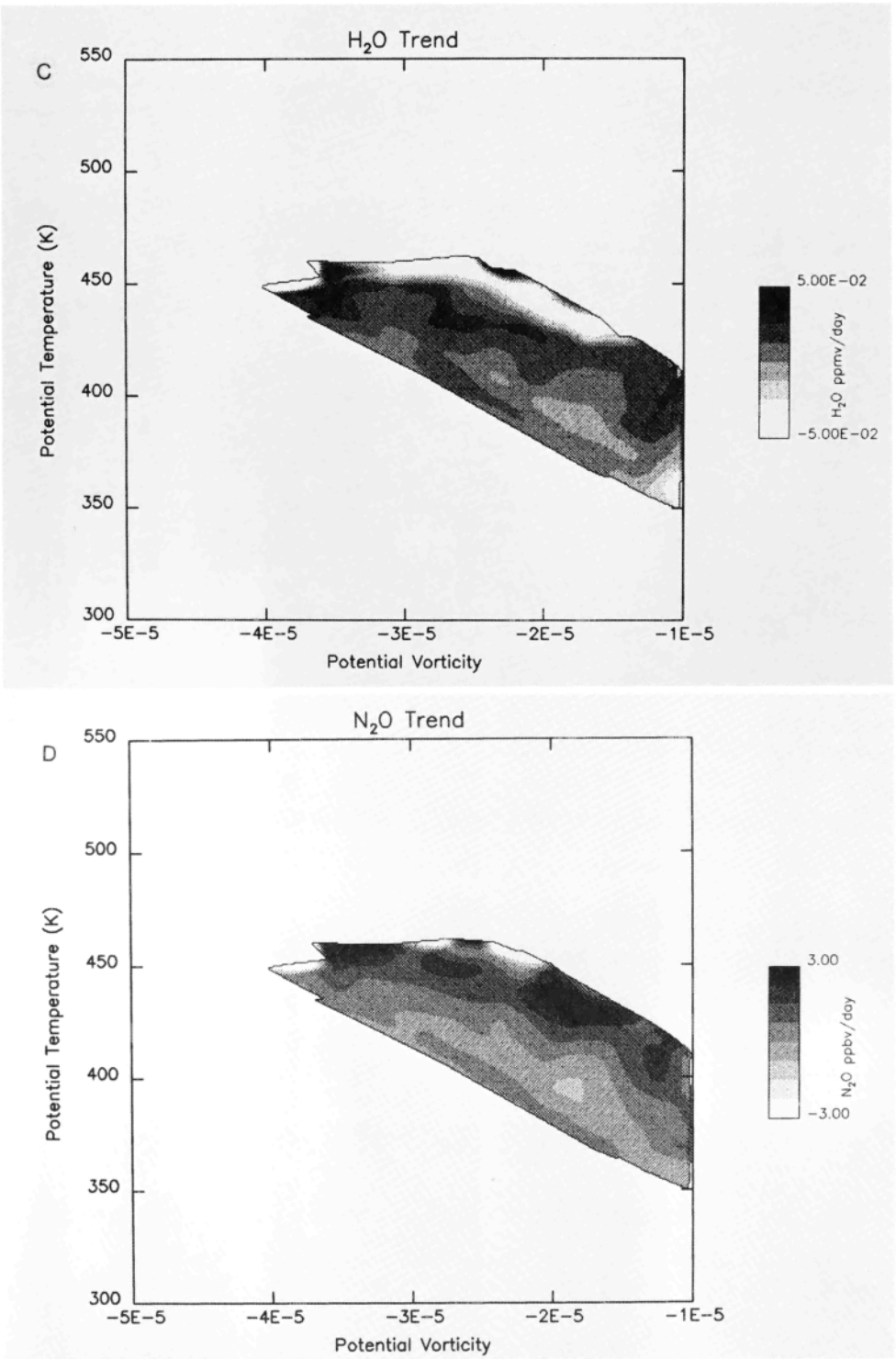

Fig. 9. (continued)

species along a PV or N_2O contour. Further observations will be required to assess the relative importance of these sources of variance.

The transforms into the (PT, N_2O) and (PT, PV) reference frames show that ozone changes inside the polar vortex or CPR are due to chemical processes, and these chemical changes are taking place in the region of high ClO. Ozone decreases at the rate of about 0.06 ppmv/d in this region. These results are in agreement with the conclusions of *Anderson et al.* [1989] and straightforward analysis of the ER-2 dive data within the CPR. Thus while the coordinate transformations increase our confidence in the conclusions drawn directly from the aircraft data, they do not alter the basic results.

The transform of ClO into conservative coordinates shows that this species changes very slowly over the mission period, although some increase is noted. ClO is not the only reservoir of active chlorine, so this change may result from

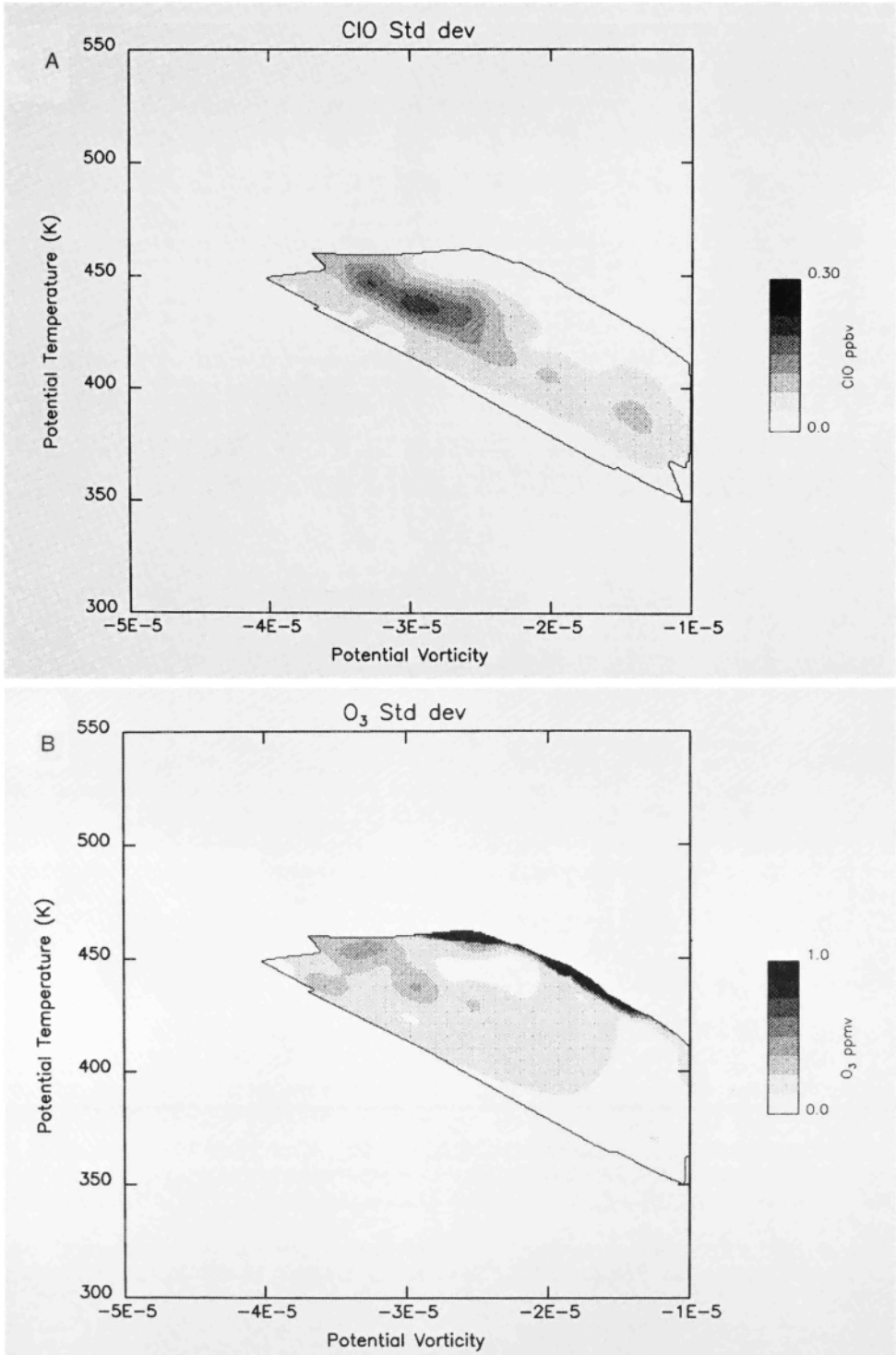

Fig. 10. The time rms deviation of the observations shown in Figures 8 and 9.

the repartitioning of active chlorine or further conversion from the reservoirs $ClONO_2$ and HCl. Transforms into (PT, PV) coordinates show that N_2O is principally a function of PV and therefore makes a good surrogate for PV during this period [see *Hartmann et al.*, 1989]. N_2O trends are negligible within the CPR; thus the diabatic cooling rate must be less than 0.2 K/d near 20 km. However, trends in ozone and N_2O outside the CPR at the highest levels suggest the presence of diabatic cooling of a magnitude of 0.3–0.6 K/d. At lower levels outside the CPR, observations suggest weak diabatic heating.

Using the data in the (PT, PV) reference frame, reconstructions of the N_2O, O_3, H_2O, and ClO fields can be generated. Results for the last three mission days (September 20–22, 1987) were compared with observations. Generally, the reconstructions show good agreement with the flight observations, except that sharp species gradients are smoothed in the reconstructions. The N_2O distribution is

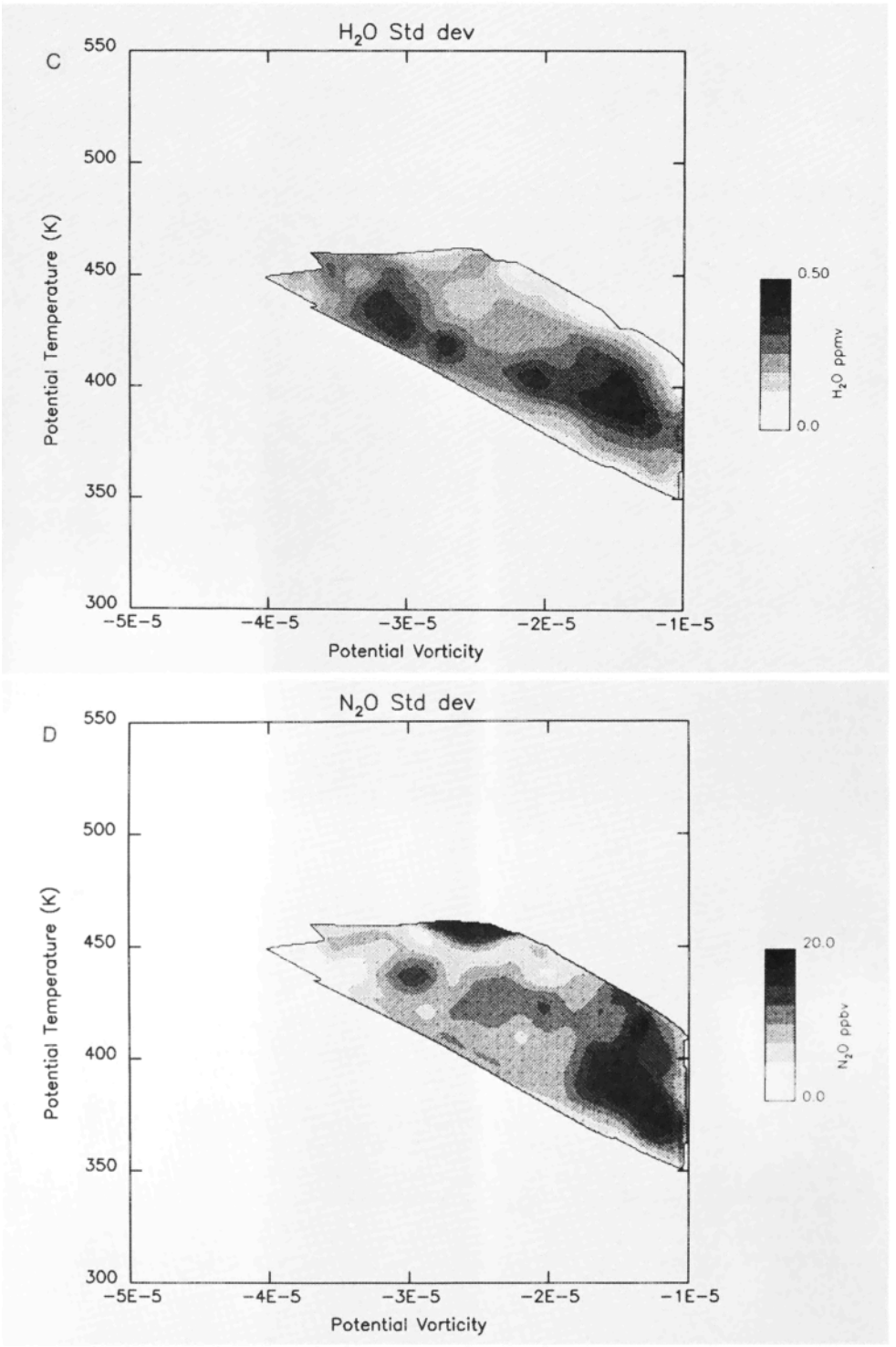

Fig. 10. (continued)

seen to be strongly depressed within the CPR, and the lowest ozone values are collocated with the region of high ClO. The meteorological observations of the last three mission days show that the polar vortex moves toward South America from September 20, 1987, to September 23, 1987. The reconstructed species concentrations generally reflect that movement, with ClO concentrations increasing at lower latitudes and altitudes.

The (PT, PV) and (PT, N_2O) coordinate transformations and reconstruction technique provides a powerful tool for interpreting the chemical structure of the vortex from limited observations in a highly variable meteorological field. In effect, the method synthesizes knowledge about the meteorological field in a way to extend limited information about the constituent fields. The technique is not limited to aircraft observations; balloonsonde data or other remote measurements can be easily incorporated into the (PT, PV) data base.

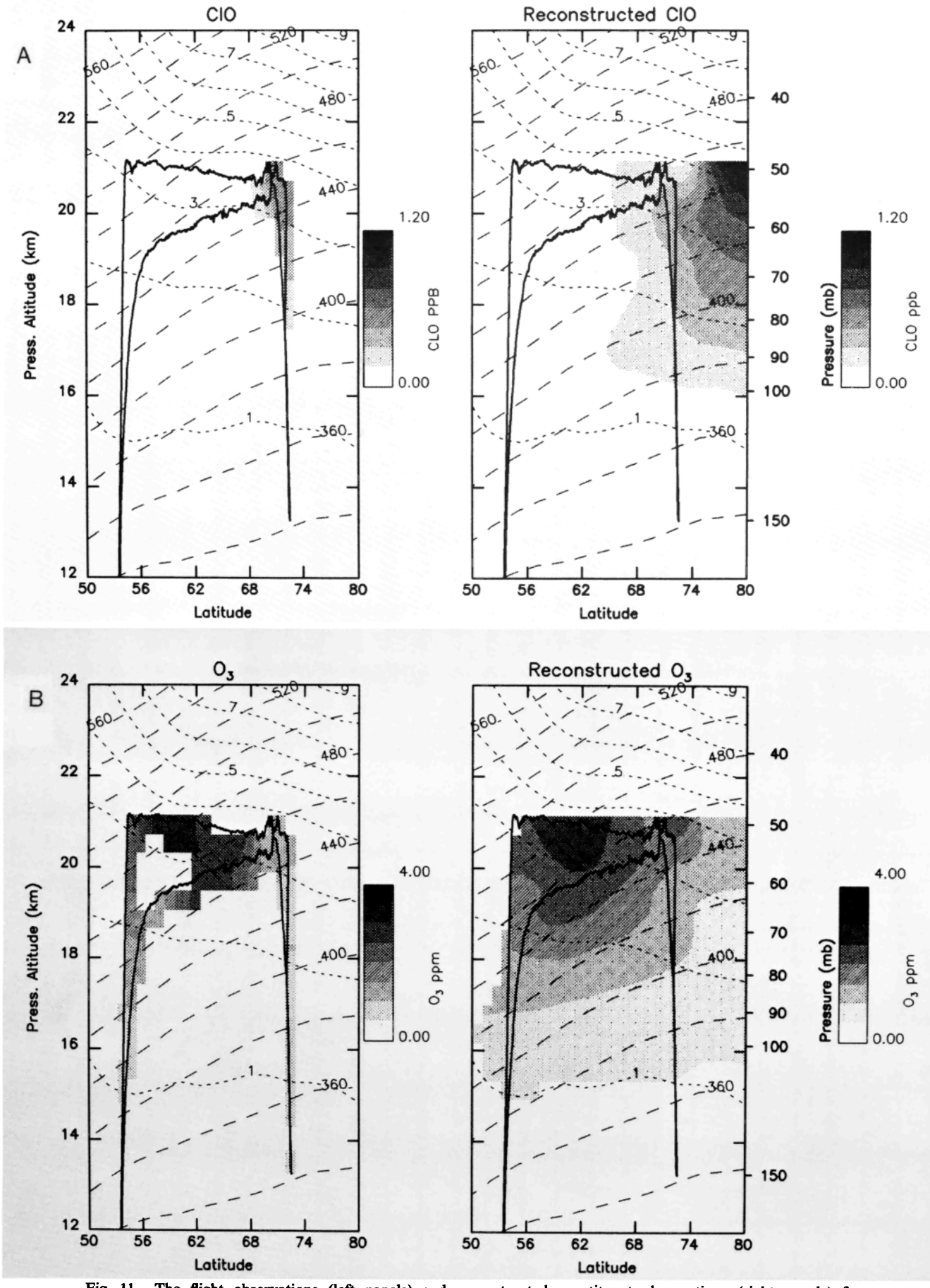

Fig. 11. The flight observations (left panels) and reconstructed constituent observations (right panels) for September 20, 1987: (*a*) ClO, (*b*) O_3, (*c*) H_2O, and (*d*) N_2O. The flight track is represented by a solid line in both panels. Left panel shows the 65°W potential vorticity (dotted lines), potential temperature (dashed lines), and the flight track (solid line) (see Figure 2*e*–2*h*).

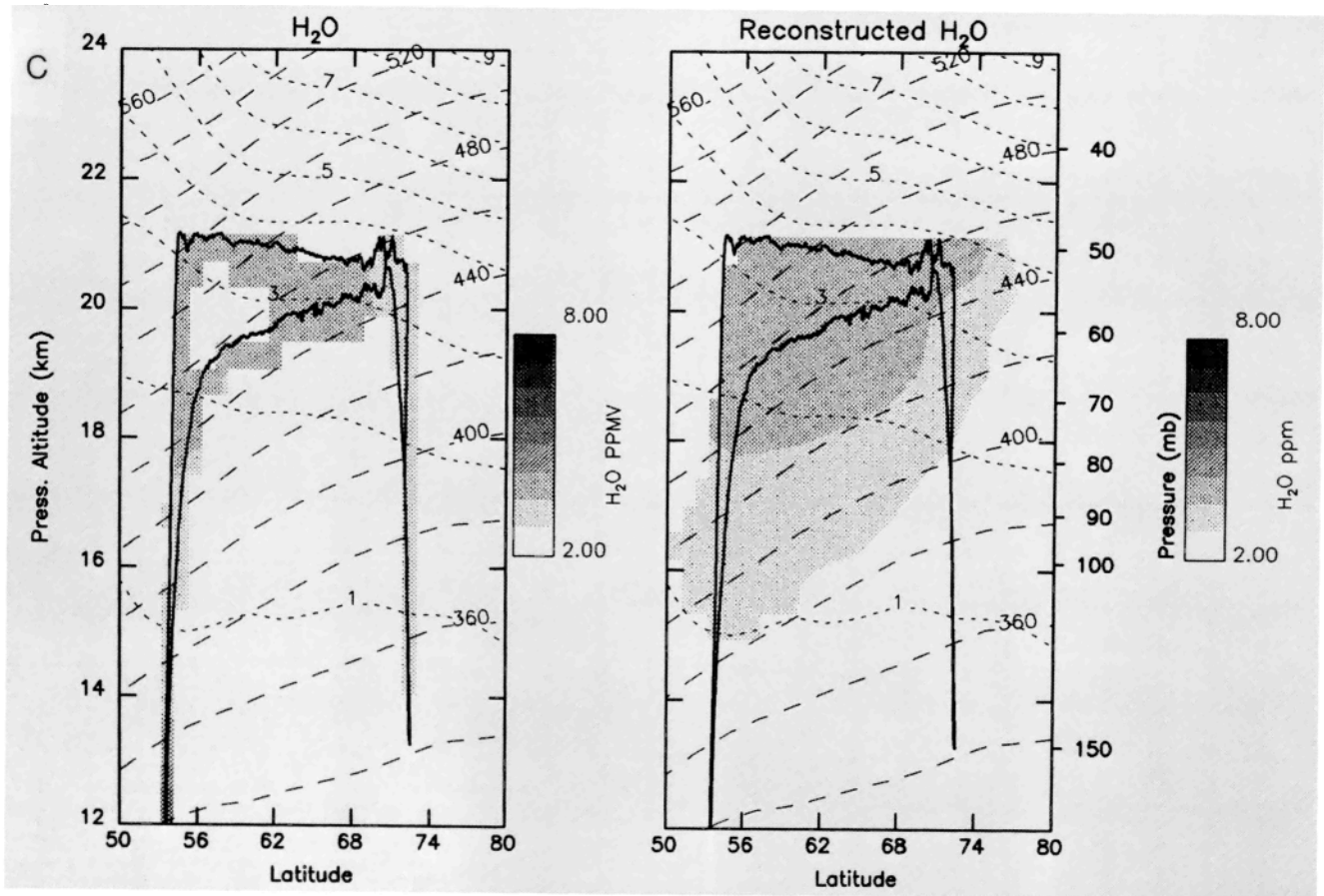

Fig. 11. (continued)

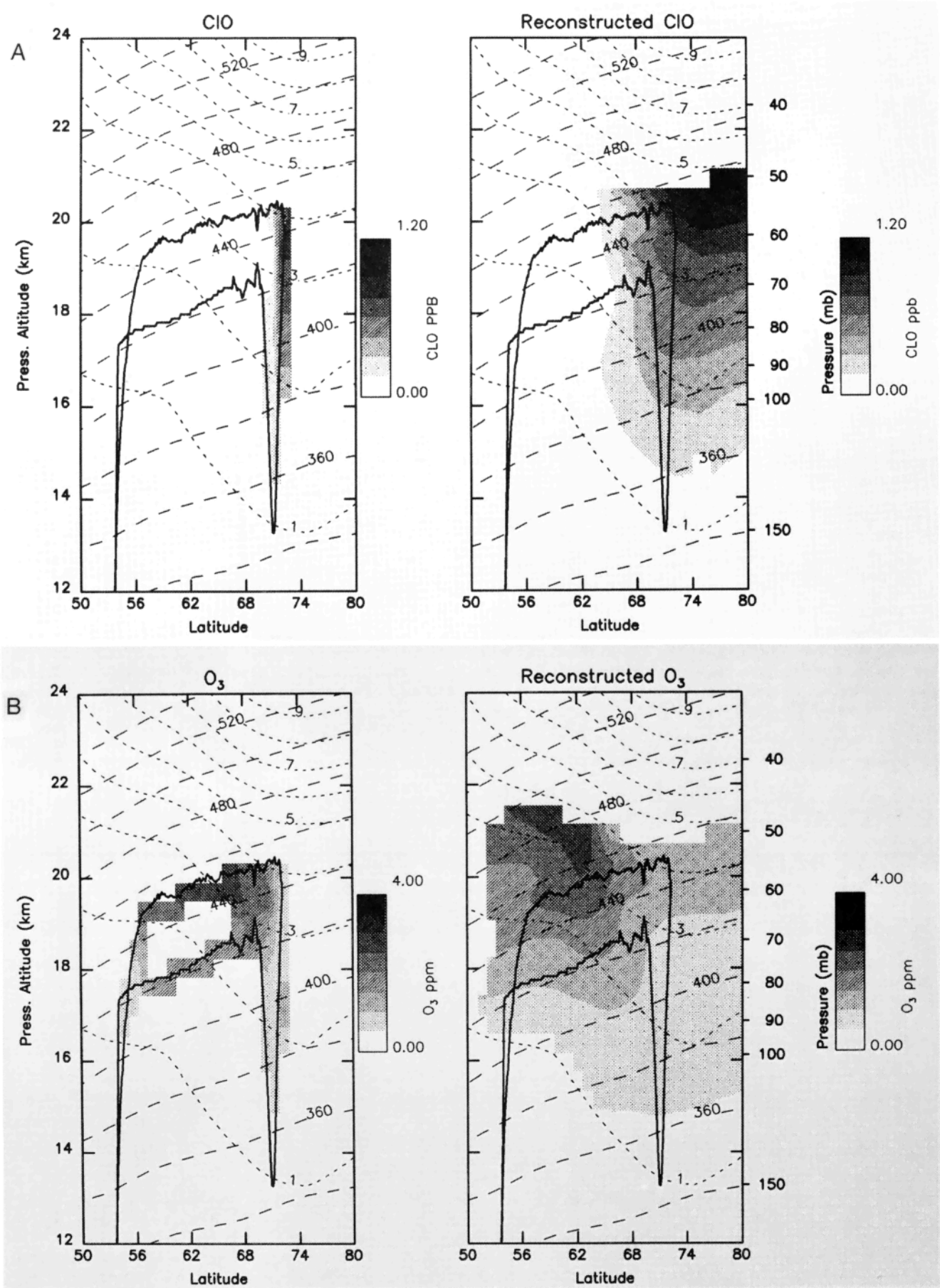

Fig. 12. Same as Figure 11 except for September 21, 1987.

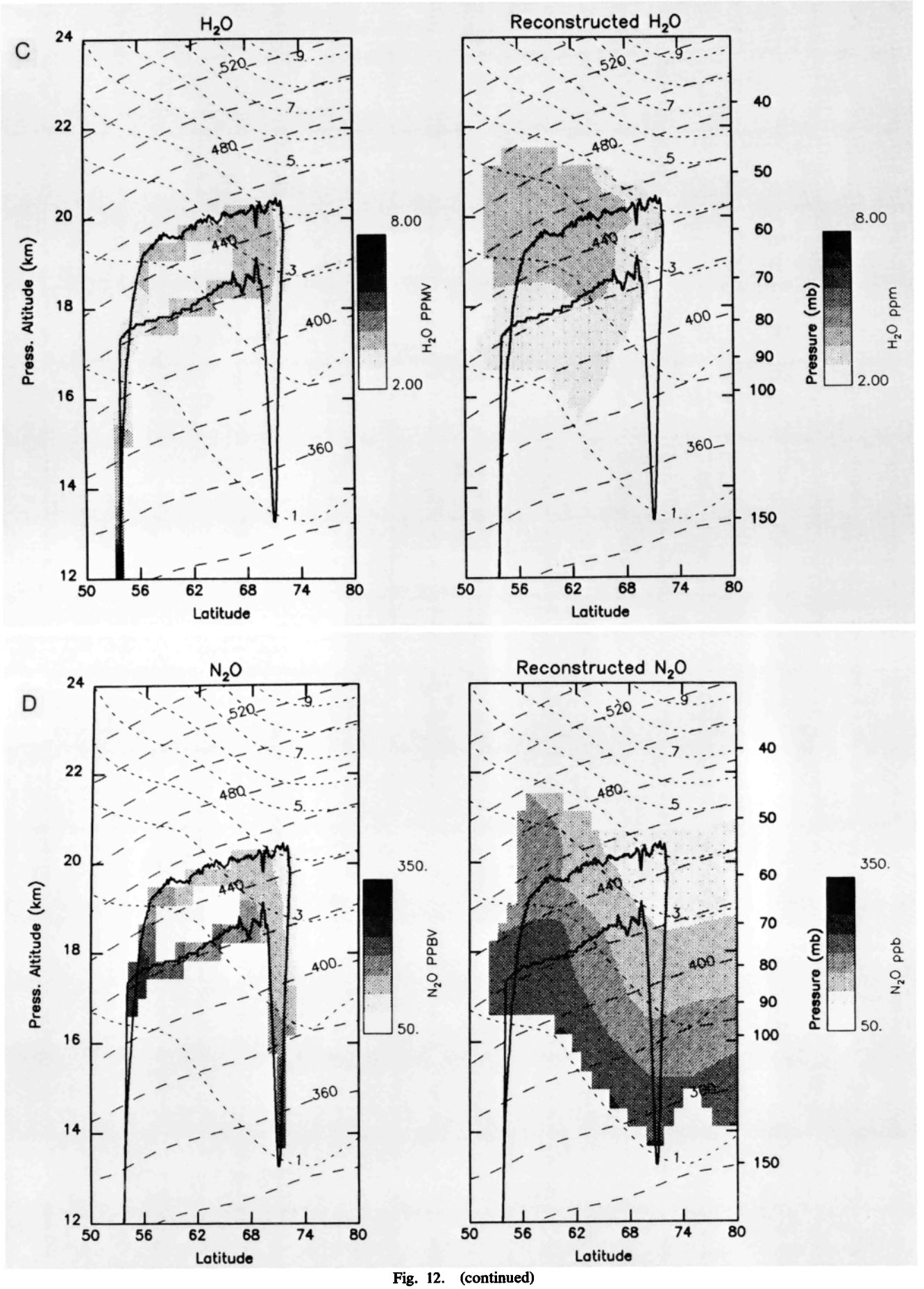

Fig. 12. (continued)

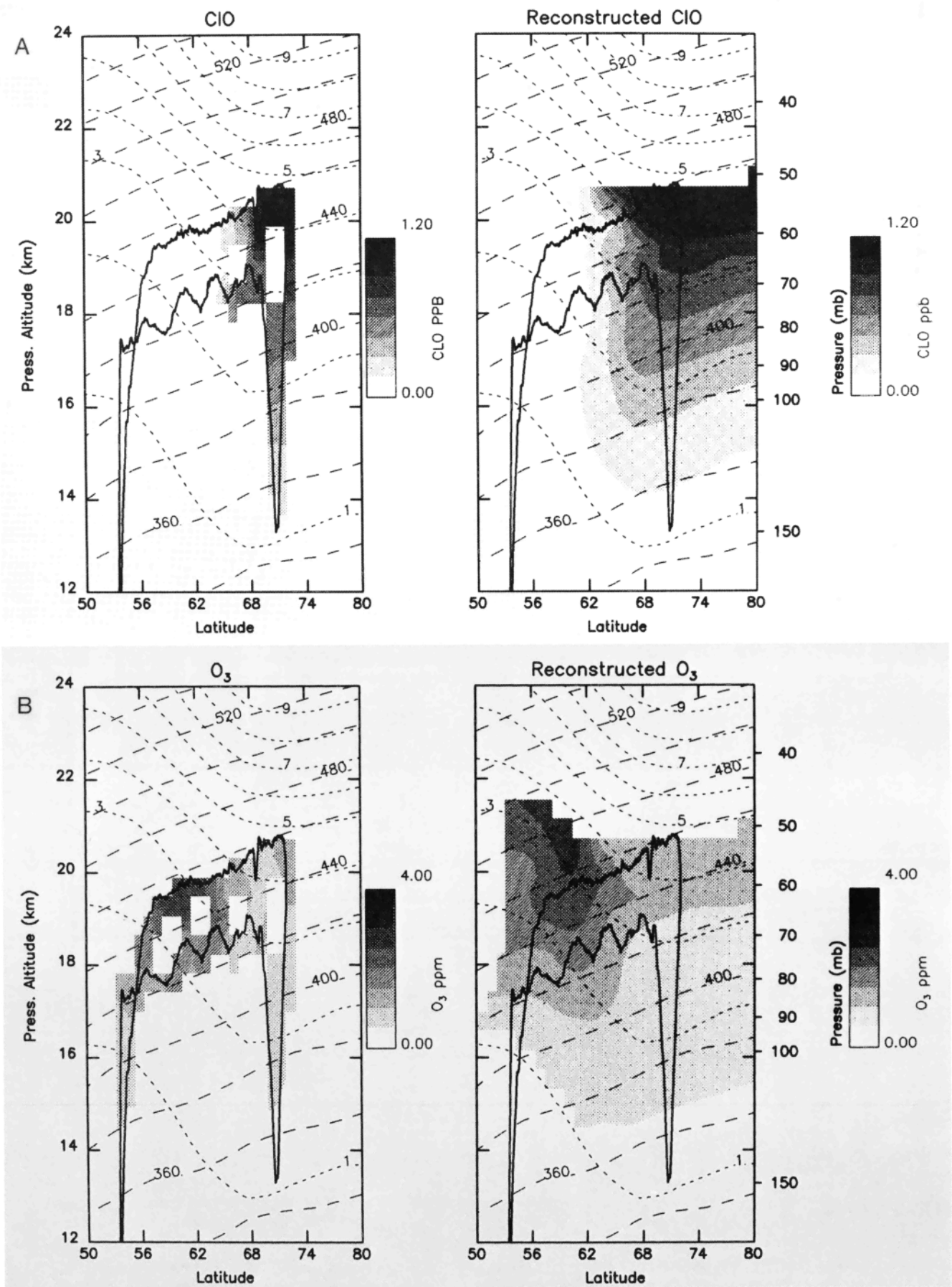

Fig. 13. Same as Figure 11 except for September 22, 1987.

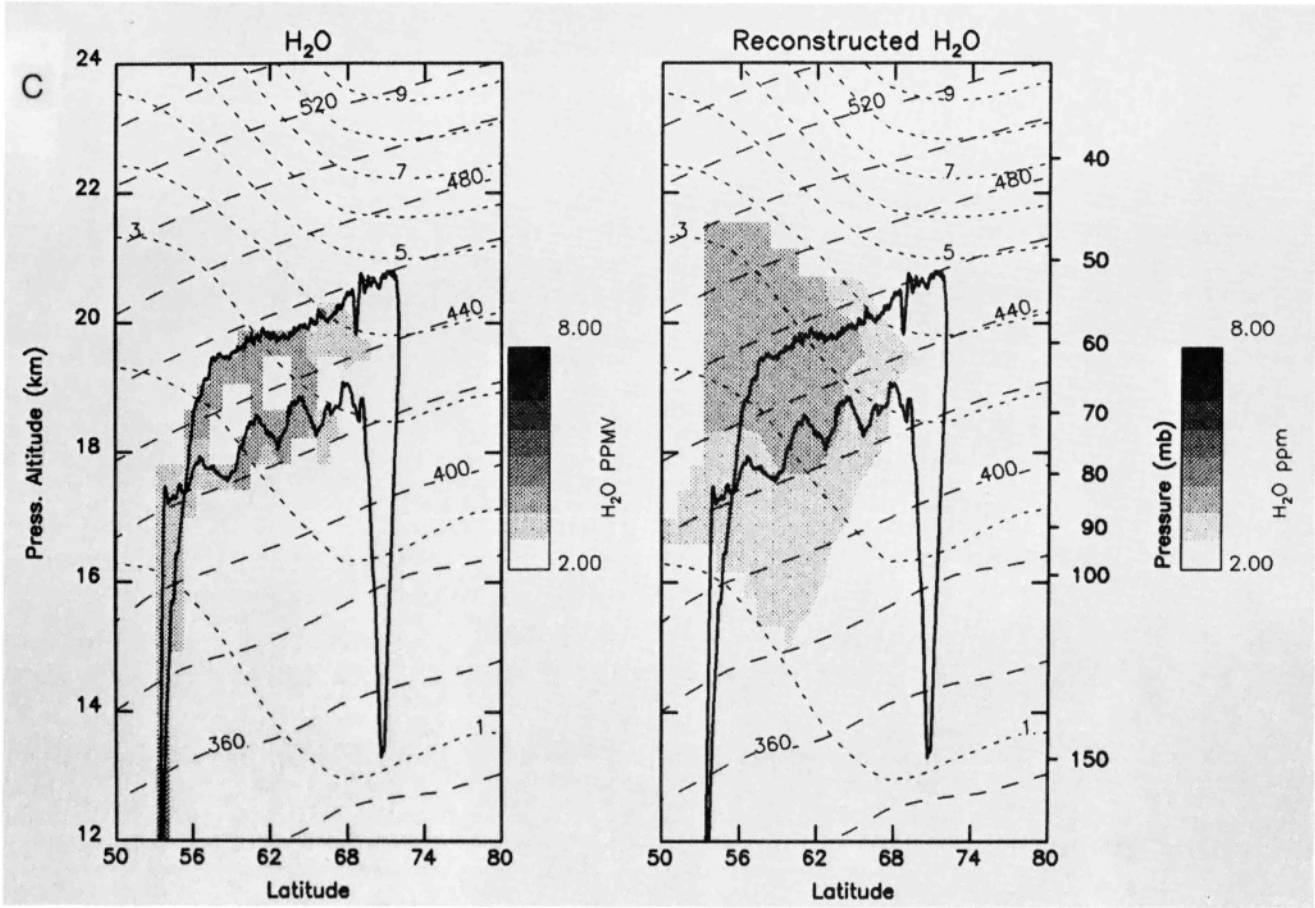

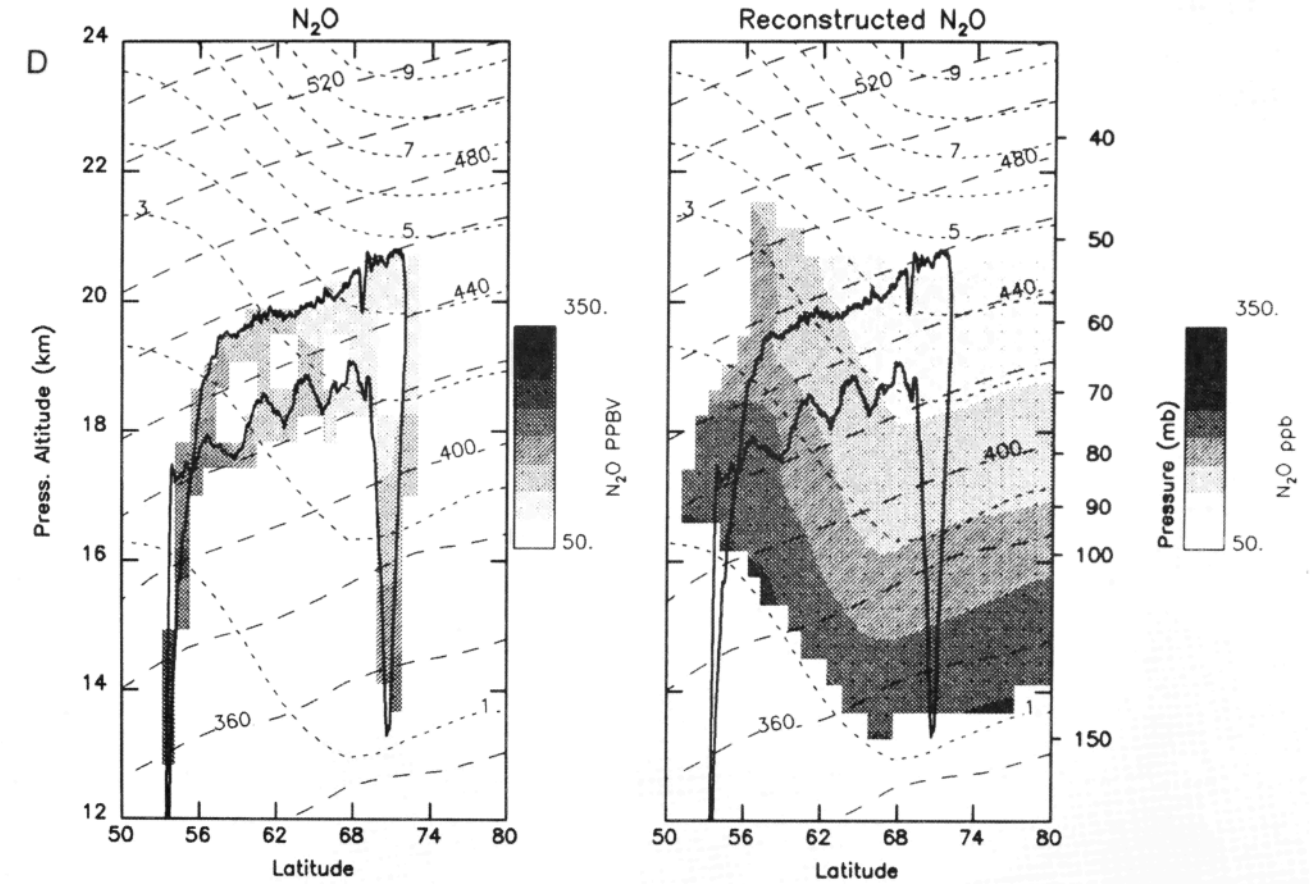

Fig. 13. (continued)

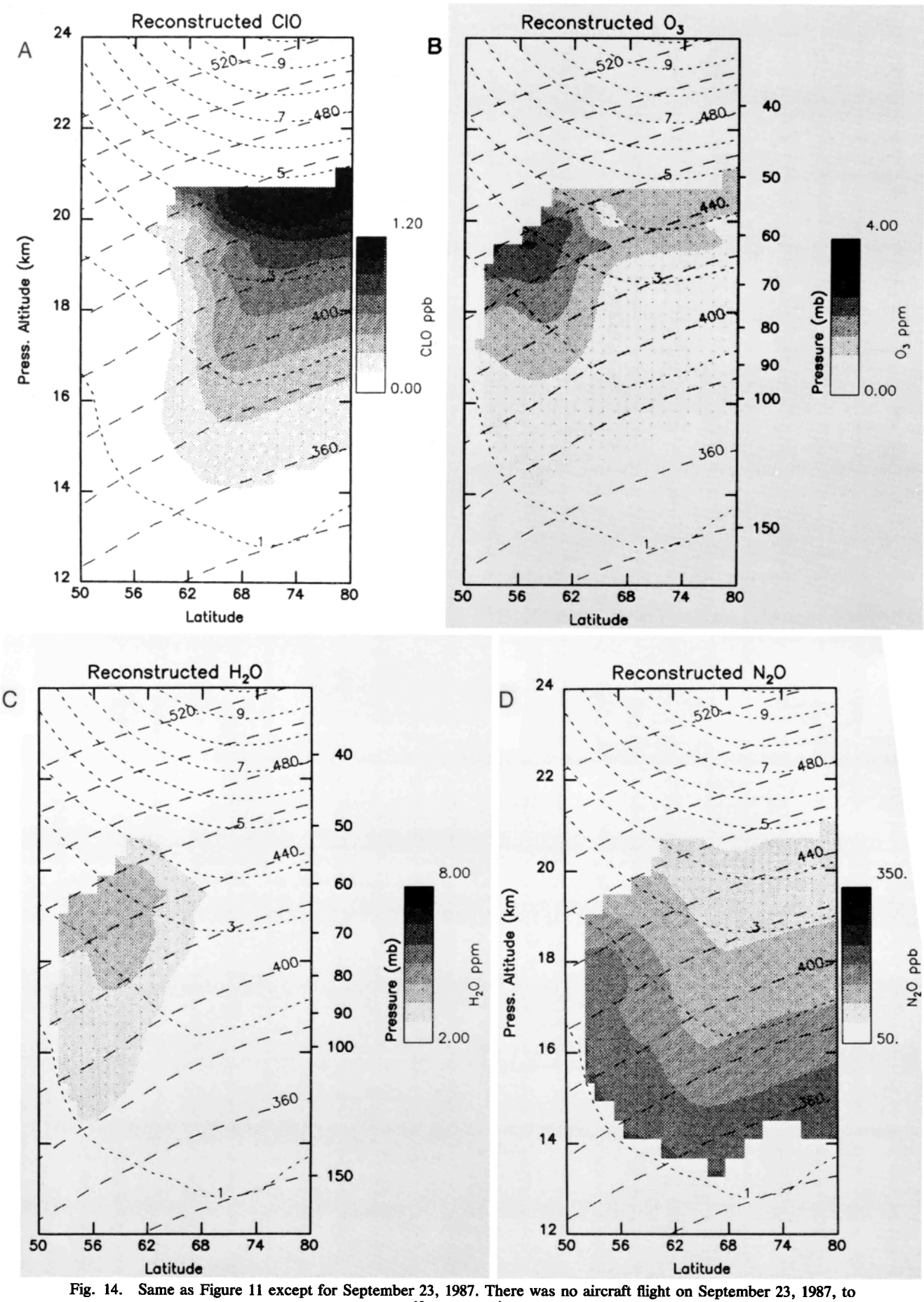

Fig. 14. Same as Figure 11 except for September 23, 1987. There was no aircraft flight on September 23, 1987, to verify computations.

APPENDIX A. FLIGHT TRACK AND NMC POTENTIAL VORTICITY COMPUTATIONS

The computations of potential vorticity along the flight track were performed independent of those reported by *Hartmann et al.* [1989], although the overall results were found to be similar. The method used here is described below.

The definition of potential vorticity is

$$\mathrm{PV} = -g\partial\theta/\partial p(-\partial u/\partial x + \partial v/\partial y + f) \qquad \text{(A1)}$$

or, in spherical coordinates,

$$\mathrm{PV} = -g\partial\theta/\partial p[(-\cos(\phi)\partial u/\partial\phi + \sin(\phi)u + \partial v/\partial\lambda)/(a\cos(\phi) + f] \qquad \text{(A2)}$$

where ϕ is latitude, λ is longitude, u is zonal wind, v is meridional wind, a is radius of the Earth, $dx = a\cos(\phi)\,d\lambda$, $dy = ad\phi$, g is acceleration due to gravity, p is pressure, θ is potential temperature, and f = planetary vorticity = $2\Omega\sin(\phi)$, where Ω is the frequency of the Earth's rotation [see *Andrews et al.*, 1987].

Latitude, longitude, and winds were measured by the Meteorological Measurement System (MMS), while $\partial\theta/\partial p$ was obtained from the lapse rates measured by the Microwave Temperature Profiler (MTP). In order to remove the shear contribution due to small-scale gravity waves, the measurements were smoothed by applying successive boxcar averages of length 160, 80, 40, 6, and 3 points to each time series (the points being spaced about 10 s apart in time). The MMS instrument failed on the flight of August 23, 1987, so flight winds estimated by the ER-2 inertial navigation system and temperatures from MTP were used instead.

Because the flights were approximately in the north-south direction, and because $\partial u/\partial y \gg \partial u/\partial x$, we take $\partial u/\partial y = \Delta u/\Delta y$. The Δu and Δy were computed for each time step from the smoothed time series and combined to yield the $\partial u/\partial y$ term.

Owing to the north-south direction of the flights, as well as the fact that $\partial v/\partial x$ was not much greater than $\partial v/\partial y$, flight data could not be used for the $\partial v/\partial x$ term. Therefore $\partial v/\partial x$ was calculated entirely from NMC analyses and interpolated onto the flight track.

Where aircraft takeoff and dives occur, an appreciable portion of the Δu comes from $\partial u/\partial z$, and $\partial u/\partial y$ can no longer be approximated by $\Delta u/\Delta y$. In those regions, computations of potential vorticity from NMC analyses are interpolated to the flight track. (Linear interpolation is used in the horizontal, and cubic spline interpolation in $\log p$ coordinates is used in the vertical.) The NMC values are often slightly offset from the flight-computed PV values, so both data sets are blended smoothly over the region where substitution occurs, to form a single continuous data series.

The NMC potential vorticity computations follow those described by *Newman et al.* [1988] except that balanced winds are used [see *Randel*, 1987]. The use of balanced winds near the pole provides better agreement with flight observations.

The NMC and flight PV generally compare well, with the flight PV picking up finer spatial detail. The rms deviation between the two is approximately $3.2e-6$ K m/s^3/Pa, or 12% of the average PV value. An exception is the flight of August 23, 1987, in which the flight PV is offset from the NMC PV by approximately $10.0e-6$ K m/s^3/Pa over portions of the flight; this date's PV therefore was not used in our analyses.

APPENDIX B. RECONSTRUCTION OF CONSTITUENT FIELDS

For each flight which contains a dive, the points at which a constituent was measured were located in terms of PV and PT along the flight track; PV was computed as in Appendix A. The flight track in both (PT, N_2O) and (PT, PV) space forms three sides of a trapezoidlike structure. Interior to the edges of the trapezoid flight envelope, the constituent values were linearly interpolated in two dimensions. This results in a constituent field in that space sampled every $1.1e-7$ K m/s^3/Pa in PV and 0.68 K in PT. These daily fields were then smoothed in both directions with a boxcar average whose width was $1.6e-6$ K m/s^3/Pa and 10.1 K, respectively.

For each point in the (PT, PV) space thus created, a time series was constructed of the constituent values at that point. Where at least one point existed in the time series, a mean field was computed. Where two or more points existed, a trend was calculated (for more than two points, this was done with a linear least squares fit). The constituent field in (PT, PV) space for any given day during the mission could then be reconstructed using these mean and trend values. In addition, each point in (PT, PV) space was tagged with the first and last days for which there were constituent measurements at that point. A point's time series was used in a day's field only if the day was inside or not more than 2 days outside the ends of that point's time series. Thus undue extrapolation in time was avoided.

The constituent field in (PT, PV) space for a given day, as determined from the mean and trend, were then inverse transformed (reconstructed) back into real (longitude-latitude-height) space using that day's NMC analyses for PV and PT: for each location in real space for which a constituent value was desired, values of PV and PT at and near this location were obtained from the NMC analyses by three-dimensional linear interpolation. The ranges of PV and PT formed by these values generate a trapezoid in (PT, PV) space. The constituent field located within this region was read and averaged, and this average was taken as the constituent value at the desired location.

REFERENCES

Anderson, J. G., W. H. Brune, and M. H. Proffitt, Ozone destruction by chlorine radicals within the Antarctic vortex: The spatial and temporal evolution of ClO-O_3 anticorrelation based on in situ ER-2 data, *J. Geophys. Res.*, *94*, 11,465–11,479, 1989.

Andrews, D. G., and M. E. McIntyre, An exact theory of nonlinear waves on a Lagrangian-mean flow, *J. Fluid Mech.*, *89*, 609–646, 1978.

Andrews, D. G., J. R. Holton, and C. B. Leovy, *Middle Atmosphere Dynamics*, 489 pp., Academic, San Diego, Calif., 1987.

Brasseur, G., and S. Solomon, *Aeronomy of the Middle Atmosphere*, 452 pp., D. Reidel, Hingham, Mass., 1986.

Brune, W. H., J. G. Anderson, and K. R. Chan, In situ observations of BrO over Antarctica: ER-2 aircraft results from 54°S to 72°S latitude, *J. Geophys. Res.*, this issue.

Butchart, N., Evidence for planetary wave breaking from satellite data: The relative roles of diabatic effects and irreversible mixing, in *Transport Processes in the Middle Atmosphere*, edited by G. Visconti and R. Garcia, pp. 121–136, D. Reidel, Hingham, Mass., 1987.

Butchart, N., and E. Remsberg, The area of the stratospheric polar

vortex as a diagnostic for tracer transport on an isentropic surface, *J. Atmos. Sci.*, *43*, 1319–1339, 1986.

De Zafra, R. L., M. Jaramillo, A. Parrish, P. Solomon, B. Connor, and J. Barrett, High concentration of chlorine monoxide at low altitudes in the Antarctic spring stratosphere: Diurnal variations, *Nature*, *328*, 408–411, 1987.

Dunkerton, T. J., C.-P. Hsu, and M. E. McIntyre, Some Eulerian and Lagrangian diagnostics for a model stratospheric warming, *J. Atmos. Sci.*, *38*, 819–843, 1981.

Hartmann, D. L., K. R. Chan, B. L. Gary, M. R. Schoeberl, P. A. Newman, R. L. Martin, M. Loewenstein, J. R. Podolske, and S. E. Strahan, Potential vorticity and mixing in the south polar vortex during spring, *J. Geophys. Res.*, *94*, 11,625–11,640, 1989.

Hartmann, D. L., L. E. Heidt, M. Loewenstein, J. R. Podolske, J. Vedder, W. L. Starr, and S. E. Strahan, Transport into the south polar vortex in early spring, *J. Geophys. Res.*, this issue.

Juckes, M. N., and M. E. McIntyre, A high-resolution one-layer model of breaking planetary waves in the stratosphere, *Nature*, *328*, 590–596, 1987.

Kelly, K. K., A. F. Tuck, D. M. Murphy, M. H. Proffitt, D. W. Fahey, R. L. Jones, D. S. McKenna, M. Loewenstein, J. R. Podolske, S. E. Strahan, G. V. Ferry, K. R. Chan, J. F. Vedder, G. L. Gregory, W. D. Hypes, M. P. McCormick, E. V. Browell, and L. E. Heidt, Dehydration in the lower Antarctic stratosphere during late winter and early spring, 1987, *J. Geophys. Res.*, *94*, 11,317–11,357, 1989.

Kohmyr, W. D., S. J. Oltmans, and R. D. Grass, Atmospheric ozone at South Pole, Antarctica, *J. Geophys. Res.*, *93*, 5167–5184, 1988.

Leovy, C. B., C.-R. Sun, M. H. Hitchmann, E. E. Remsberg, J. M. Russell III, L. L. Gordley, J. C. Gille, and L. V. Lyjak, Transport of ozone in the middle stratosphere: Evidence for planetary wave breaking, *J. Atmos. Sci.*, *42*, 230–244, 1985.

Mahlman, J. D., and S. B. Fels, Antarctic ozone decrease: A dynamical cause?, *Geophys. Res. Lett.*, *13*, 1316–1319, 1986.

McIntyre, M. E., Towards a Lagrangian-mean description of stratospheric circulations and chemical transports, *Philos. Trans. R. Soc. London, Ser. A*, *296*, 129–148, 1980.

McIntyre, M. E., On the Antarctic ozone hole, *J. Atmos. Terr. Phys.*, *51*, 29–43, 1988.

McIntyre, M. E., and T. N. Palmer, Breaking planetary waves in the stratosphere, *Nature*, *305*, 593–600, 1983.

Newman, P. A., D. J. Lamich, M. Gelman, M. R. Schoeberl, W. Baker, and A. Krueger, Meteorological atlas of the southern hemisphere lower stratosphere for August and September, *NASA Tech. Memo 4049*, 1988.

Podolske, J. R., M. Loewenstein, S. E. Strahan, and K. R. Chan, Stratospheric nitrous oxide in the southern hemisphere, *J. Geophys. Res.*, this issue.

Proffitt, M. H., J. A. Powell, A. F. Tuck, D. W. Fahey, K. K. Kelly, A. J. Krueger, M. R. Schoeberl, B. L. Gary, J. J. Margitan, K. R. Chan, M. Loewenstein, and J. R. Podolske, A chemical definition of the boundary of the Antarctic ozone hole, *J. Geophys. Res.*, *94*, 11,437–11,448, 1989.

Proffitt, M. H., M. J. Steinkamp, J. A. Powell, R. J. McLaughlin, O. A. Mills, A. L. Schmeltekopf, T. L. Thompson, A. F. Tuck, T. Tyler, R. H. Winkler, and K. R. Chan, In situ measurements within the 1987 Antarctic ozone hole from a high-latitude ER-2 aircraft, *J. Geophys. Res.*, this issue (*a*).

Proffitt, M. H., K. K. Kelly, J. A. Powell, B. L. Gary, M. Loewenstein, J. R. Podolske, S. E. Strahan, and K. R. Chan, Evidence for diabatic cooling and poleward transport within and around the 1987 Antarctic ozone hole, *J. Geophys. Res.*, this issue (*b*).

Randel, W. J., The evaluation of winds from geopotential height data in the stratosphere, *J. Atmos. Sci.*, *44*, 3097–3120, 1987.

Rosenfield, J. E., M. R. Schoeberl, and M. A. Geller, A computation of the stratospheric diabatic circulation using an accurate radiative transfer model, *J. Atmos. Sci.*, *44*, 859–876, 1987.

Rosenfield, J. R., M. R. Schoeberl, and P. A. Newman, Antarctic springtime ozone depletion computed from temperature observations, *J. Geophys. Res.*, *93*, 3833–3849, 1988.

Shine, K. P., On the modelled thermal response of the Antarctic stratosphere to a depletion in ozone, *Geophys. Res. Lett.*, *13*, 1331–1334, 1986.

Solomon, S., The mystery of the Antarctic ozone "hole," *Rev. Geophys.*, *26*, 131–150, 1988.

Solomon, S., G. H. Mount, R. W. Sanders, and A. L. Schmeltekopf, Visible spectroscopy at McMurdo Station, Antarctica, 2, Observations of OClO, *J. Geophys. Res.*, *92*, 8329–8338, 1987.

Tung, K. K., On the relationship between the thermal structure of the stratosphere and the seasonal distribution of ozone, *Geophys. Res. Lett.*, *13*, 1308–1311, 1986.

J. Anderson, Harvard University, Cambridge, MA 02138.

K. R. Chan, M. Loewenstein, J. Podolske, and S. E. Strahan, NASA Ames Research Center, Moffett Field, CA 94035.

B. Gary, Jet Propulsion Laboratory, Pasadena, CA 91109.

D. L. Hartmann, Department of Atmospheric Sciences, University of Washington, Seattle, WA 98195.

P. A. Newman and R. L. Martin, Applied Research Corporation, Landover, MD 20785.

M. H. Proffitt, NOAA Aeronomy Laboratory, Boulder, CO 80303.

M. R. Schoeberl and L. R. Lait, NASA Goddard Space Flight Center, Greenbelt, MD 20771.

(Received May 24, 1988;
revised May 18, 1989;
accepted May 18, 1989.)